american physiological society

JNP JOURNAL OF NEUROPHYSIOLOGY

J Neurophysiol 135: 1499–1517, 2026.
First published April 10, 2026; doi:10.1152/jn.00070.2025

RESEARCH ARTICLE

Control of Movement

Rigid control of motor unit firing rates in the human tibialis anterior muscle persists during neurofeedback

Meng-Jung Lee,[1,2] Patrick Ofner,[1,2] Hsien-Yung Huang,[3,7] Joris Mulder,[4] Jaime Ibañez,[5,6] Dario Farina,[7] and Carsten Mehring[1,2,8]

[1]*Bernstein Center Freiburg, University of Freiburg, Freiburg im Breisgau, Germany;* [2]*Faculty of Biology, University of Freiburg, Freiburg im Breisgau, Germany;* [3]*Department of Engineering and Design, University of Sussex, Brighton, United Kingdom;* [4]*Department of Methodology and Statistics, Tilburg University, Tilburg, The Netherlands;* [5]*Centro de Investigacion Biomedica en Red en Bioingeniera, Biomateriales y Nanomedicina, CIBER, Zaragoza, Spain;* [6]*BSICoS, I3A and IIS Aragón, Universidad de Zaragoza, Zaragoza, Spain;* [7]*Department of Bioengineering, Imperial College London, London, United Kingdom; and* [8]*BrainLinks-BrainTools, University of Freiburg, Freiburg im Breisgau, Germany*

Abstract

The conventional framework of motor unit (MU) control assumes that MUs in a MU pool are constrained by a fixed recruitment order and a common input. This rigid control framework has been challenged by recent findings suggesting that MU activity could be flexibly modulated, potentially mediated by descending cortical inputs. In this study, rather than evaluating flexibility from the perspective of recruitment thresholds, we investigated control flexibility by assessing whether human participants can voluntarily modulate MU firing rates beyond rigid control constraints. Specifically, we examined whether participants could voluntarily modulate the firing rates of a pair of MUs from the tibialis anterior muscle during real-time feedback. Two tasks involving target reach with different visual feedback derived from the MUs' firing rates were conducted. In both tasks, there was no evidence that participants were able to change MU firing rates in a way that would violate rigid control robustly. Our findings demonstrate limited flexibility in MU control in human tibialis anterior muscle within single-session training, even when real-time MU activity feedback was provided. The results suggest that MU flexibility is not inherently present in the human lower limb.

NEW & NOTEWORTHY How flexibly can the central nervous system control individual motor units? We tested whether humans can achieve independent control of pairs of motor units from the tibialis anterior muscle in two experiments with real-time visual feedback of motor unit firing rates. The results of both experiments provided no evidence of independent control.

common synaptic input; flexible control; motor unit; neurofeedback

INTRODUCTION

Motor units (MUs) are fundamental functional units through which the nervous system controls movement (1). Flexible MU control could potentially provide a control signal for neural interface applications with more than a single degree of freedom (DoF) per muscle (2). A noninvasive approach has been developed to decompose high-density surface electromyography (HD-sEMG) signals, enabling the real-time acquisition of multiple MU activities simultaneously (3–6). Despite the potentially numerous DoFs available with MUs, studies have shown that the central nervous system employs various strategies to reduce its computational load (7–9), effectively limiting the DoF. MUs are orderly recruited on the basis of their intrinsic neural properties according to Henneman's size principle (10–12), which has been observed robustly in various muscles (13–17). Additionally, activities of MUs within the same functional group (18–20) are highly correlated because of the large portion of common input they receive (21–24). Such a rigid control scheme proposes that the activity of each MU changes in a predictable way dependent on the common input. In this framework one would expect that the firing rates of any two MUs in a single-compartment muscle within the same pool

Correspondence: C. Mehring (carsten.mehring@biologie.uni-freiburg.de).
Submitted 28 July 2025 / Revised 22 September 2025 / Accepted 1 March 2026

0022-3077/26 Copyright © 2026 The Authors. Licensed under Creative Commons Attribution CC-BY 4.0.
Published by the American Physiological Society.

Downloaded from journals.physiology.org/journal/jn (062.036.043.138) on June 24, 2026.

are confined to a one-dimensional curve (a 1-dimensional manifold) in the two-dimensional space spanned by their firing rates (state space) (25), imposing constraints on the voluntary control of the individual MUs (26, 27).

Though the recruitment order of MUs appears to be fixed, reversals in recruitment order can be observed in certain cases such as during fast force changes (25, 28, 29). Selective activation of single MUs at different recruitment thresholds within the same muscle has also been reported with biofeedback training (30–32). Furthermore, in macaque monkeys cortical microstimulation and MU activity during dynamic force profiles revealed deviations from activity patterns typically observed during slow force ramp tasks, consistent with the presence of multiple descending neural pathways enabling selective cortical control of MUs (25). However, a recent study in humans showed that participants could only achieve selective control of MUs within a muscle by leveraging the recruitment-derecruitment hysteresis, without providing any evidence for voluntary selective control of the input to MUs (26). Given that recruitment order can be influenced by factors such as contraction speed (25), muscle length (33), and posture (34), a change of the recruitment order does not necessarily indicate flexible control of individual MUs (1, 28). Therefore, a more robust approach, such as assessing firing rate modulation while excluding recruitment and derecruitment considerations, is desirable to determine whether MUs can be flexibly controlled. However, as of yet it remains unclear whether MU firing rates can be voluntarily and flexibly modulated while they are steadily active, i.e., recruited.

In this study, we therefore investigated the flexibility in controlling MU firing rates in the human tibialis anterior muscle. Unlike previous studies that examined changes in recruitment order, we focused exclusively on continuously recruited MUs to avoid the effect of MU recruitment and derecruitment. If MUs can be controlled independently through descending neural signals, their firing rates should not be restricted monotonically to the common drive during activation regardless of their recruitment thresholds. To assess flexible MU control, we borrowed the concept of "displacement zone" introduced by Marshall et al. (25) (see Fig. 3*A*). The term displacement zone refers to the deviation of the firing rates of two MUs from a one-dimensional manifold within the two-dimensional state space. Firing rates of MUs can only fall within the displacement zone if the firing rates of the two MUs change simultaneously in opposite directions. Such behavior cannot be achieved through one source of common input and thus would indicate flexible MU control.

Two single-session target-reaching tasks, namely displacement control and difference control, were conducted. Real-time visual feedback of the MU firing rates was provided via a cursor on a computer screen (see Fig. 1), with each task employing a distinct mapping of firing rates to cursor movement. In the displacement control task, the cursor position along the x-/y-axes was controlled by the firing rates of the MU pair. In the difference control task, participants were provided with a less restrictive control condition with an alternative mapping of MU firing rates to the cursor position. No evidence was found to support that participants could consistently modulate MU firing rates into the displacement zones in either task.

MATERIALS AND METHODS

Participants

In total 33 able-bodied participants were recruited for this study. Ten participants carried out the displacement control task (1 female and 9 males, aged 23–33 yr), and 21 participants carried out the difference control task (11 females and 10 males, aged 21–39 yr). Two more participants were recruited but did not perform any task because the MU decomposition quality was initially insufficient to continue the experiment. None of the participants took part in both tasks. Four participants in the difference control task (among them 2 authors of this study) were exposed to similar but not identical experimental paradigms before their participation. The remaining participants had no such prior experience. The study was approved by the institutional ethics committees of the University of Freiburg (approval number 21–1388-1), and all participants gave their written informed consent before starting the experiment.

One participant's data in the difference control task were not recorded during the baseline phase because of an oversight in the data collection protocol. For this reason, this participant's data were excluded from all neural analyses but included in all behavioral analyses. In addition, only participants with sufficient MU decomposition quality throughout the entire recording session were included in the analysis in the main results (details are provided in *Decomposition Stability and Exclusion of Participants*). Thus, in total 9 participants from the displacement control task (1 female and 8 males) and 10 participants from the difference control task (5 females and 5 males; 2 of them being authors of this study) were included in the main analyses.

Experimental Setup and Data Acquisition

Figure 1 illustrates the experimental setup. HD-sEMG signals were acquired from the tibialis anterior muscle of the self-reported dominant leg over the muscle belly aligned to the fiber direction with a 64-channel surface electrode grid (1-mm electrode diameter, 8-mm interelectrode distance; GR08MM1305; OT Bioelettronica, Torino, Italy) with a 64-channel adapter (AD64F; OT Bioelettronica). Before the electrode grid was applied, the area of the skin was shaved. The surface of the skin was then cleaned with an abrasive gel (EVERI; Spes Medical Srl, Genova, Italy) and subsequently with water to remove any residual gel. A self-adhesive foam layer (FOA08MM1305; OT Bioelettronica) was placed onto the electrode grid, and conductive paste (AC Cream; Spes Medical Srl) was applied between the skin and the electrode grid. After the electrode grid was placed, medical adhesive tape was used to ensure the fixation of the grid on the leg. In addition, bipolar sEMGs from the fibularis longus (FL) and the lateral and medial heads of the gastrocnemius muscle (GL and GM) were recorded with disposable adhesive surface electrodes (24 mm, CDES000024; Spes Medical Srl). All sEMG signals were filtered with a 10- to 500-Hz, 4th-order Butterworth band-pass filter and sampled at 2,048 Hz with a Quattrocento Amplifier system (OT Bioelettronica).

Downloaded from journals.physiology.org/journal/jn (062.036.043.138) on June 24, 2026.

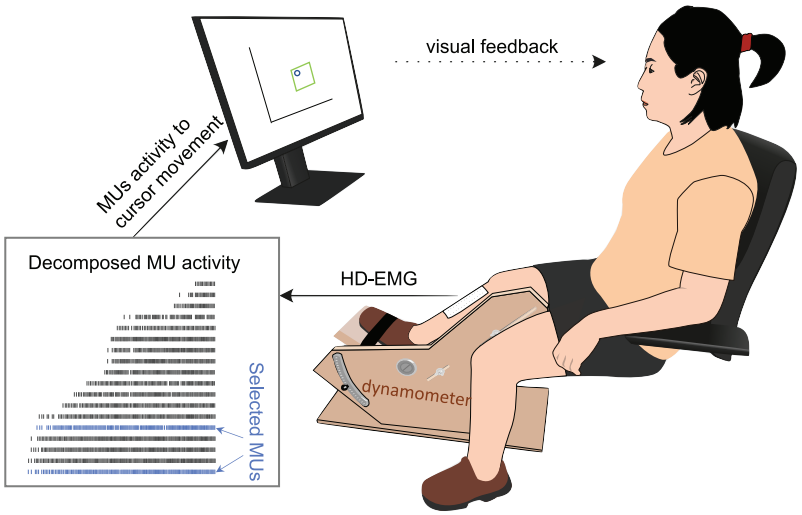


Figure 1. Schematic overview of the experimental setup. The participant's foot from the dominant leg was secured to the dynamometer with Velcro. A 1-dimensional force sensor on the dynamometer measured the force exerted by the dorsiflexion movement. High-density surface electromyographic signals (HD-EMG) from the tibialis anterior muscle were obtained and decomposed into motor unit (MU) activities in real time. A pair of MUs were selected as controlled MUs. The activities of the controlled MUs were translated into cursor movement that was presented to the participant on a screen.

The force exerted by the dorsiflexion movement on the dominant leg was measured with an ankle dynamometer (NEG1; OT Bioelettronica) with a positioning system and a single-degree of freedom force transducer. The participant placed the dominant leg onto the dynamometer at a 90° angle of the ankle, and the participant's foot was fixed to the dynamometer with a hook-and-loop tape. The recorded force signal was amplified and low-pass filtered at 33 Hz with a preamplifier (Forza; OT Bioelettronica) and then recorded with the Quattrocento amplifier. The communication between the amplifier and the computer was implemented with buffers of data packages consisting of 128 samples, corresponding to 62.5 ms.

Experimental Paradigm

In the beginning of the experiment, the participants' dorsiflexion force was measured during maximum voluntary contraction (MVC). Afterward, the participants completed a few trapezoidal force profiles to familiarize themselves with the setup and feedback. This was followed by a single trapezoidal profile to calibrate the MU decomposition. Subsequently, participants performed force tasks and proceeded to the MU control task (displacement or difference control). After the control task they repeated the force and MVC tasks. Further details are provided in the following subsections.

Preexperimental calibration.

To measure the MVC force level, participants were first asked to perform a maximum isometric dorsiflexion of the ankle three times for 5 s each time, interrupted by a 15-s break. The maximum measured force from the dynamometer was then used to determine the MVC force level and served as a reference force for the rest of the experiment. During the following tasks in the preexperimental calibration, the instantaneous force produced by isometric dorsiflexion was presented to participants on a computer screen in front of them, together with a force profile that they were supposed to follow. At first, participants were asked to follow a trapezoidal profile (*trapezoid I*: 10-s ramp-up from 0% to 10% MVC, 20-s hold at 10% MVC, 10-s ramp-down from 10% to 0% MVC) for two to five repetitions as a familiarization to this type of force tracking task. Participants then tracked a second trapezoidal force profile with a longer hold period once (*trapezoid II*: 10-s ramp-up, 30-s hold at 10% MVC, 10-s ramp-down). A motor unit (MU) decomposition algorithm (35) was calibrated with the HD-sEMG signals recorded during the *trapezoid II* profile. In the later stages of the experiment (see below), this decomposition algorithm was applied to obtain MU spiking activities in real time (4, 26) from the HD-sEMG signals. At the end of the calibration sessions, the participants were asked to track the *trapezoid I* profile one more time. The force-to-firing rate relationships, as well as the spike-triggered averages of the HD-sEMG signals, were obtained from these data and used for MU selection (see below).

Force tracking tasks.

After the preexperimental calibration, participants performed three repetitions of the *trapezoid I* force tracking task, with 10-s rest between repetitions. This set of three repetitions was performed again after the control tasks (see below) to assess changes in MU properties, such as recruitment and derecruitment thresholds, and to assess decomposition quality. Recruitment thresholds were defined as the average force values within a 200-ms window centered on the first instance of MU firing rates exceeding 5 Hz during ramp-up, whereas the derecruitment thresholds were defined using the average force values within a 200-ms window but centered at the instance of when the firing rate dropped to 0 Hz during ramp-down (1). Recruitment and derecruitment thresholds were determined for each trapezoid separately and then averaged across the three repetitions.

Those participants who would later carry out the displacement control task additionally tracked three chirp force profiles after the *trapezoid I* force tracking task. The amplitude of these force profiles was 2% MVC, and they were centered at 3%, 4%, and 5% MVC. For all chirp profiles the instantaneous frequency increased linearly from 0.1 Hz to 1.3 Hz during the first 30 s, and during the subsequent 30 s it decreased linearly from 1.3 Hz to 0.1 Hz. Visual feedback of the applied force was provided throughout the task. The chirp profiles were recorded with the intention to investigate whether MU

Downloaded from journals.physiology.org/journal/jn (062.036.043.138) on June 24, 2026.

activities generated during the displacement task, which are indicative of flexible control, could also be generated during dynamic force modulation. Since our results did not suggest flexible MU control during the displacement task, the chirp recordings were not further analyzed here.

MU selection.

The MUs used for control in the displacement and difference control tasks were selected as follows. Participants controlled the vertical position of a cursor on a screen in front of them by the sum of the firing rates of two MUs. The horizontal position of the cursor was fixed. One or two circular areas were shown on the screen (for the difference and displacement control tasks, respectively), reflecting the baseline areas later used in the respective tasks (see below). Participants were asked to repeatedly move the cursor into the indicated circle, during which the experimenter selected two MUs from the available MU pool. The MU selection was based on the following criteria:

1) The recruitment thresholds of the two selected MUs should be as low as possible, preferably below 5% MVC. MUs with lower recruitment thresholds were preferentially selected to minimize the risk of fatigue during the experiment.
2) The two selected MUs should have similar recruitment thresholds (to avoid the scenario in which one MU has reached its peak firing rate while the other was just being recruited).
3) MUs with more regular spiking, i.e., with a smaller coefficient of variation of interspike intervals (ISIs), during the hold phase of the force tracking task were preferred, as irregular firing can indicate lower MU decomposition quality.
4) If more than two MUs met *criteria 1–3* equally well, an MU pair with a similar range of firing rates across various force levels was selected.

After the two control MUs were selected, the MU with the lower recruitment threshold during the single repeat *trapezoid I* profile done at the end of the calibration sessions was assigned as MU_1 and the one with higher recruitment threshold MU as MU_2. Additional gain factors for each MU were manually set. The gain factors functioned as multipliers to the firing rates to ensure similar adjusted firing ranges of the two MUs. This was crucial for the displacement control task because the baseline area was centered along the diagonal of the firing rate state space. In the difference control experiment, ensuring similar firing rates after gain adjustment was important to minimize cursor movement along the horizontal axis once the cursor movement in the horizontal direction was unlocked at the beginning of the action phase. For both MUs, gain-adjusted firing rates between 7 and 9 Hz were targeted when reaching the baseline area in the difference control task. The gain factor ratio MU_1/MU_2 was 0.98 ± 0.03 (mean ± SD) for the displacement control task and 0.97 ± 0.09 (mean ± SD) for the difference control task.

Displacement control task.

In this task, participants controlled a cursor on the screen in front of them with the gain-adjusted firing rates from two MUs, MU_1 and MU_2. The firing rate of MU_1 controlled the horizontal cursor position (along the *x*-axis), while the firing rate of MU_2 controlled the vertical cursor position (along the *y*-axis). The cursor position was updated at the end of each data package.

The single-session experiment comprised five blocks and a total of 200 trials. Each block included 40 trials, with 10 trials per target per block, and the targets were presented in a random order. Each trial consisted of two phases: the baseline phase and the action phase (see Fig. 3*C*). To initiate a trial, participants had to move the cursor over the baseline area and hold it in the baseline area for 3 s. The holding time was indicated by a circular timer surrounding the baseline area. During the 3-s hold phase, the cursor was required to remain within the baseline area. If it left the baseline for >1 consecutive second, the timer was reset to zero. The baseline areas (gray) were represented by circles of 2-Hz radii centered at 6 Hz/6 Hz (*area A*) and 8 Hz/8 Hz (*area B*) (see Fig. 3*B*). When the baseline phase ended, the circle showing the baseline area disappeared, and the trial entered the action phase. Baseline firing rates were determined by averaging firing rates across the 3-s holding phase, and these baseline firing rates were used to set the position of the subsequent target. Targets appeared as a square box with a side length of 5 Hz with their upper left vertex [for target (*T*)*1* and *T3*] or their lower right vertex (for *T2* and *T4*) at the average baseline firing rate (see Fig. 3*B*). As a consequence, the targets visualized the displacement areas with regard to the baseline firing rates, as illustrated in Fig. 3*A*. In each trial, either *T1* or *T2* followed baseline *area A*, whereas either *T3* or *T4* was presented after baseline *area B*. The participants were given 10 s to move and hold the cursor in the target area for as long as possible. Participants received a reward of 10 points and a coin-earning sound each time the cursor remained within the target for 125 ms. The total number of points that participants had obtained was displayed at the top of the screen. In addition, two red bars were positioned along the *x*- and *y*- axes. The cursor touched the bars if one MU was derecruited, and participants received an immediate penalty of minus 50 points upon contact with the bars. Subsequent penalties were applied only if the cursor remained over the bar for an additional 600 ms or longer. If at any time during the action phase both MUs were derecruited simultaneously, the current trial was discontinued. A 5-s break occurred between the individual trials within a block and a 2-min break between the individual blocks.

We did not include targets on the manifold that could be reached by mere force modulation. Although such targets may provide a baseline for learning, their inclusion would have reduced the available training time for the used displacement targets *T1–T4*.

Difference control task.

In this task, the vertical cursor position was controlled by the sum of the firing rates of MU_1 and MU_2, whereas the horizontal cursor velocity was controlled by the difference of the firing rates (see Fig. 8*A*). The cursor position was updated at the end of each data package. Firing rate differences needed to exceed a threshold to generate a

Downloaded from journals.physiology.org/journal/jn (062.036.043.138) on June 24, 2026.

nonzero velocity. The x-position of the cursor (x_t) was computed as

$$x_t = x_{t-1} + \left(g^{(1)}\lambda_t^{(1)} - g^{(2)}\lambda_t^{(2)}\right) \text{if} \left| \frac{g^{(1)}\lambda_t^{(1)} - g^{(2)}\lambda_t^{(2)}}{g^{(1)}\lambda_t^{(1)} + g^{(2)}\lambda_t^{(2)}} \right| > 0.05$$

where t is the time step, x_t is the x-position of the cursor at time t, $g^{(1)}$, $g^{(2)}$ are the gain factors for MU_1 and MU_2, and $\lambda_t^{(1)}, \lambda_t^{(2)}$ are the firing rates of MU_1 and MU_2 at time t. If the absolute difference of the gain-adjusted firing rates was not above the threshold (0.05), the velocity was set to 0 to reduce noisy cursor movements. The cursor position along the y-axis was set to the sum of the gain-adjusted firing rates, i.e., $y_t = g^{(1)}\lambda_t^{(1)} + g^{(2)}\lambda_t^{(2)}$, where y_t is the y-position of the cursor at time t.

The single-session experiment comprised five blocks and a total of 180 trials. Each block included 36 trials, with 18 trials per target presented in a random order. Participants engaged in a food delivery game involving two sequential steps in each trial (Supplemental Fig. S1a): *1*) Baseline phase: Participants picked up the delivery by holding the cursor (in hand shape) over the pick-up area for 1 consecutive second. The cursor could only move vertically during the baseline phase. A circular timer surrounding the pick-up area indicated the passage of time. *2*) Action phase: Once the baseline phase was successfully completed (the delivery was picked up), the participants proceeded by delivering the designated item (cursor) to one of the two houses (targets). The target house was denoted by a thought bubble appearing in the top right corner of the house (see Supplemental Fig. S1a). During the action phase, the participants were asked to keep both MUs active throughout the trial. The states of the two MUs were indicated by two traffic lights on the screen, with green and gray indicating an active and an inactive state, respectively. The cursor would only move when both MUs were active, to discourage MU derecruitment. The cursor would stop moving if one of the MUs was derecruited, and the trial would be discontinued when both MUs were derecruited. When the cursor entered the target, a circular timer surrounding the target house appeared, to signify successful target reach and indicate the duration for which the cursor was held within the target. In each trial, the action phase was limited to a maximum duration of 30 s, during which participants needed to hold the cursor within the target for 3 consecutive seconds for a trial to be considered successful. A trial was discontinued once the target was reached successfully. Upon success, the participants were awarded a score of 100 points, accompanied by a coin-earning sound. If one MU was derecruited during the 3-s holding period over the target, the timer around the target would be reset to zero so that a trial could only be successful without MU derecruitment during the hold period. Between trials, there was a 5-s pause followed by a 3-s countdown to allow participants to prepare for the next trial. In addition, there were 2-min breaks between the individual blocks.

Note that we present the results from the displacement control task first in RESULTS, although the experiments involving the displacement control task were conducted chronologically after the experiments involving the difference control task.

Decomposition Stability and Exclusion of Participants

The HD-sEMG decomposition algorithm used in this study has previously been validated and shown to yield accurate decomposition when compared to intramuscular recordings (35). We performed a systematic offline analysis of the decomposition stability in our experiments and excluded participants from further analysis when at least one of the two control MUs exhibited insufficient decomposition stability. The following measures were used to assess decomposition stability of a motor unit.

Pulse trains.

The decomposition algorithm iteratively computes motor unit-specific separation vectors onto which the HD-sEMG signals are projected to obtain the motor unit pulse trains. The discharge times of a motor unit are then acquired by k-means clustering (with $k = 2$) of the peaks of the squared motor unit pulse train (pp^2) (35). Separation vectors and cluster parameters were obtained from the recordings during a trapezoid force profile in the preexperimental calibration phase (referred to here as the decomposition ramp). A silhouette measure (SIL) was computed to evaluate the consistency of the clustering, and only motor units with SIL > 0.9 for the data from the decomposition ramp were used (35). The separation vectors and cluster parameters obtained from the decomposition ramp were used in the control blocks to obtain MU spike trains from HD-sEMG recordings online.

Nonstationarities during subsequent recordings can lead to degrading cluster separability over time and thus wrong cluster assignment of new incoming data during online experiments. As a consequence, actual action potentials may be missed (false negatives) or be detected where there are none (false positives). To assess the stability of cluster separability, we reapplied the k-means clustering algorithm offline after the experiments to the recordings during the control blocks. Here, k-means was applied separately to the data from each block to obtain individual cluster thresholds that were optimized for each block. See Supplemental Figs. S8a and S9a for units from two participants with low and high stability, respectively. Occasional extreme pp^2 values were removed before performing k-means offline, using a threshold of five times the median of the pp^2 values from action potentials classified during the decomposition ramp. For participants included in the main results, the MUs used for control had SIL values obtained from offline clustering exceeding 0.89 across all control blocks.

Even if cluster separability remains high, nonstationarities in the HD-sEMG signals can result in reduced pp^2 peak values and thus shifts of the action potential cluster to lower values (Supplemental Fig. S8a in contrast to Supplemental Fig. S9a). In such situations, a static cluster threshold as used in the online experiments can lead to missed spikes. We compared the spike trains obtained after reapplication of k-means to the spike trains obtained online and computed the fraction of missed spikes under the assumption that the spike trains obtained after reapplication of k-means reflect the ground truth (Supplemental Figs. S8c and S9c, blue lines). This estimate may overstate the number of missed spikes due to false positives in the clustering after reapplication,

Downloaded from journals.physiology.org/journal/jn (062.036.043.138) on June 24, 2026.

for example resulting from decreased cluster separability. For the participant shown in Supplemental Fig. S8a this is reflected in the less separable clusters in later blocks. To improve the estimate of missed spikes, we introduced the relative interspike interval (rISI), which measures the duration of an ISI in relation to the median duration of adjacent ISIs:

$$\mathrm{rISI}_n = \frac{\mathrm{ISI}_n}{\mathrm{med}(X)} \text{ with } X = \{\mathrm{ISI}_{n-\Delta}, \mathrm{ISI}_{n-\Delta+1}, \ldots, \mathrm{ISI}_{n+\Delta}\}$$

Here, n indexes the sequence of ISIs across the recording and Δ specifies the number of adjacent ISIs before and after the current ISI that are used to calculate the median ISI. Δ was set to 12 in this analysis. For slowly changing firing rates and given the regularity of MU spiking, rISI values should fluctuate around 1, whereas missed spikes would yield peaks around 2 and 3 in the rISI histograms (Supplemental Figs. S8b and S9b). We therefore estimated the fraction of missed spikes by using only those additional spikes after reapplication of *k*-means that were found in ISIs with rISI values above 1.2 or 1.5 (Supplemental Figs. S8c and S9c). This led to a slightly smaller fraction of estimated missed spikes in blocks where clusters were less separable (Supplemental Fig. S8c). If the fraction of the estimated missing spikes was too high or showed a strong increase across blocks, the participant was excluded from the analysis.

ISI histograms.

We assessed stability also by visual inspection of the ISI histograms during the control blocks. The emergence of distinct second or third peaks in the ISI histograms (see Supplemental Fig. S8d for an example and in contrast Supplemental Fig. S9d), located at two or three times the ISI of the highest peak, may also indicate the presence of missing spikes. When such distinct peaks were observed, we typically also observed a higher fraction of missed spikes according to the measure described in *Pulse trains* and therefore the participant was excluded.

Besides false negatives, false positive spike detections could also lead to incorrect estimation of firing rates. False positives could result from a degradation in decomposition quality, additional noise in the recorded EMG signal (e.g., external interference), or the conflation of signals from newly recruited MUs with those of the decomposed MUs, compromising the accuracy of the spike detection. False positives would produce an excess of short ISIs that would not be expected for the recorded MU during the used force levels and tasks. If an excess of such short ISIs was observed in the ISI histograms for the control blocks, the participant was also excluded.

We also investigated the ISI histograms from the trapezoid force profiles performed before and after the control tasks (pre and post ramps). The ISI histograms of two example participants with excess short ISIs during the pre/post ramps are shown in Supplemental Fig. S8, e and f. In the example shown in the top row of Supplemental Fig. S8e, an excess of short ISIs was observed during the hold phase of the first trapezoid (*ramp1*) of the force tracking task before the control task (ramp hold pre) and during the first and third trapezoids (*ramp1* and *ramp3*) after the control blocks (ramp hold post). However, the ISI histograms from the control blocks of the same participant (bottom row of Supplemental Fig. S8e) show no excess of short ISIs, except for a small peak during *block 1* (black arrow; note that this peak is not relevant for the control feedback as ISIs < 20 ms were excluded from firing rate estimation). Although all ramps were carried out at 10% MVC, most participants produced forces below 5% MVC during control blocks (see Fig. 4*B* and Supplemental Fig. S1d). This suggests that the short ISIs during the pre/post ramps were a result of the higher forces. Therefore, we computed ISI histograms from the ramps using only ISIs occurring during force levels up to the 99th and 90th percentiles of the force levels observed during the control blocks (Supplemental Fig. S8e). The observed decrease in the number of short ISIs with decreasing force thresholds corroborates the previous interpretation. In such cases and when in addition no excess of short ISIs was observed during the control blocks, we therefore concluded that the decomposition stability was not affected during the control blocks and did not exclude the respective participant. Conversely, if short ISIs persisted after application of lower force thresholds and/or an excess of short ISIs was observed during the control blocks (as illustrated for the unit from another participant shown in Supplemental Fig. S8f), the degradation in decomposition quality or interference from external noise was likely relevant for the control blocks, and the participant was thus excluded from the main results.

Note that the exclusion of participants did not affect our main conclusions, as Bayesian hypotheses tests using all participants also indicate that there is no evidence supporting target reach (Supplemental Fig. S5 and Supplemental Tables S4 and S5).

Supplemental Figs. S8 and S9 show the results from the analyses to assess decomposition stability of individual units from selected example participants. The analyses for both control MUs of all participants are provided in Supplemental Figs. S10–S40.

Analysis

Firing rate estimation.

Two methods were used to estimate firing rates from MU spike trains: *1*) Convolution of the MU spike trains with a 400-ms Hanning window. This method was used when determining the recruitment and derecruitment thresholds. *2*) Estimation of firing rates from interspike intervals (ISIs). This method was used to compute the MU firing rates online during the experiments with MU-controlled cursor movement. For *2*), the real-time firing rate estimate λ was updated at each new spike according to the following equation:

$$\lambda = \frac{1}{\mathrm{AVISI}_n} \text{ with } \mathrm{AVISI}_n = \alpha \times \mathrm{ISI}_n + (\alpha - 1)\mathrm{AVISI}_{n-1}$$

where ISI_n is the ISI between the current and the previous spike, AVISI_{n-1} is the weighted average of previous ISIs updated at each new spike, and n is the spike index. The current firing rate estimate λ was computed as the inverse of the last updated average ISI. The parameter α was set to 0.2. If no spike was detected for >500 ms, the firing rate was set to 0 Hz. The maximum value for AVISI_n was capped at 1,000 ms to prevent a slow increase of the firing rate estimate after a longer period of inactivity (5 s or longer). A slow firing rate increase could lead to excessive

Downloaded from journals.physiology.org/journal/jn (062.036.043.138) on June 24, 2026.

force production by the participants and thus increase the likelihood of muscle fatigue.

Removal of data points and trials.

This study focused on the continuous modulation of motor unit activities and investigated the flexibility of MU firing rate modulation while MUs were active. For this purpose, we excluded all firing rate data from the analysis within a 250-ms window centered around any period where any of the two MUs had a firing rate of 0 Hz. This approach reduced the influence of derecruitment and recruitment in the analysis. When analyzing the firing rates in the action phases, only trials that lasted longer than 3 s after the removal of the time windows were used. Out of 1,800 trials from nine participants in the displacement control experiment, a total of 1,740 trials met this criterion and were used for the analysis. In the difference control experiment, 1,589 out of 1,800 trials from 10 participants met this criterion. To assess robustness, a separate analysis of MU firing rates was conducted excluding all trials with derecruitment in one or both control MUs and using only the second half of the action phase (Supplemental Fig. S7 and Supplemental Tables S8, S9, and S10).

Determination of recruitment order for MU_1 and MU_2.

For the analyses of the difference control task, we assigned MU_1 and MU_2 in such a way that MU_1 had a lower recruitment threshold than MU_2. The recruitment order of the two units was obtained from the tracking of a trapezoidal force profile (as described above) and separately from the control tasks. For the control tasks, we used the instantaneous firing rate estimates from each individual trial and the average of the measured forces at the first occurrence of firing rates above 5 Hz, if present, as the recruitment thresholds. If the recruitment order for the control and the force tracking tasks was different, a Bayesian Wilcoxon signed-rank test was conducted to compare the recruitment thresholds obtained from the trials of the control task to the recruitment threshold obtained from the trapezoidal force profile. If the resulting Bayes factor (BF) was >10 (indicating strong evidence for a difference), the recruitment thresholds from the control task were used to determine the recruitment order of the two MUs. Otherwise, the recruitment thresholds from the trapezoidal force profile were used. Since the trapezoidal force profile is the conventional method for determining recruitment thresholds and given the higher variability of the force increase at the beginning of the control trials (the time course of the force increase was not queued but freely chosen by the participants), we only used the recruitment thresholds from the control task if there was strong evidence for a difference to the trapezoidal force task.

For the displacement control task, the recruitment order obtained from the trapezoidal force profile before the control blocks was maintained in the analysis of the main results as it reflected the visual feedback during the online experiments. A robustness analysis was performed using recruitment thresholds derived from both the trapezoidal force profile and individual control trials as described above for the difference control task. Here, the MUs were reassigned such that the recruitment threshold of MU_1 was lower than that of MU_2. The results after reassignment were consistent with those obtained when the recruitment order was not changed (Supplemental Fig. S6 and Supplemental Tables S6 and S7).

Statistics

We used Bayesian methods for hypothesis testing. The Bayes factor BF_{10} measures the level of support for comparing two hypotheses (H_1 and H_0) on a range from 0 to $+\infty$ based on data. A BF_{10} value of 1 indicates that the data do not provide evidence in favor of either H_0 or H_1, whereas a value below or above 1 provides evidence in favor of H_0 or H_1, respectively. To interpret Bayes factors, Lee and Wagenmakers (36) suggested a heuristic classification where values of BF_{10} between 1 and 3 would be considered anecdotal, values between 3 and 10 moderate, values between 10 and 30 strong, values between 30 and 100 very strong, and values above 100 extreme evidence for H_1. We applied this heuristic with a modification: any Bayes factor value > 10 was consistently interpreted as strong evidence, without further differentiation into very strong or extreme evidence. Correspondingly, for values of BF_{10} below 1, the range between 1 and 1/3 was considered anecdotal, the range between 1/3 and 1/10 moderate, and values below 1/10 strong evidence for H_0. Note that BF_{01} is given by $1/BF_{10}$.

One-sample and paired-samples designs.

For one-sample and paired-samples comparisons, we used the Bayesian Wilcoxon signed-rank test (37) implemented in JASP (https://jasp-stats.org). The default Cauchy prior with location 0 and scale $r = \frac{1}{\sqrt{2}}$ was used. To assess the robustness of the Bayes factor with regard to the prior, the Bayes factor was additionally computed for prior scales $r = 1, \sqrt{2}$ that include also wider priors. As the Bayes factor did not change qualitatively across the prior scales, we report the Bayes factor obtained with the default prior scale of $r = \frac{1}{\sqrt{2}}$ in the main text. The results for the different prior scales can be found in Supplemental Table S11.

Repeated-measures ANOVA designs.

For repeated-measures (RM) ANOVA designs, we used the Bayesian RM ANOVA implemented in JASP with random slopes (38) and the Jeffreys–Zellner–Siow prior (39). The inclusion Bayes factor ($BF_{inclusion}$) was used to assess the evidence for a predictor to be included (38, 40). We computed Bayes factors for three different prior scales for fixed effects ($r = \frac{1}{2}, \frac{1}{\sqrt{2}}, 1$), with the prior scale for random effects set to twice that of the fixed effects. As the Bayes factors were not qualitatively different across the scales, we report the Bayes factors for the default scales ($r = \frac{1}{2}$ for fixed and $r = 1$ for random effects) in the main text. The complete results for all prior scales are reported in Supplemental Table S11. Post hoc tests were conducted using the default settings for multiple comparisons in JASP, which uses a correction for multiple comparisons according to Ref. 41.

Trend analysis across blocks.

We conducted trend analyses across blocks by linear regression of the measurement (e.g., success rate) across blocks. The value for the slope coefficient obtained from the linear least-squares fit was used as a measure of the trend. We performed a Bayesian Wilcoxon signed-rank test on the

Downloaded from journals.physiology.org/journal/jn (062.036.043.138) on June 24, 2026.

obtained slopes to quantify evidence for nonzero trends. The obtained Bayes factor BF_{10}, with H_0 reflecting a slope of 0 and H_1 a slope different from 0, are reported as trend-BF_{10}. To compare trends in repeated measurements, a Bayesian repeated-measures ANOVA was applied to assess differences between slopes, with the resulting inclusion Bayes factor reported as trend-$BF_{inclusion}$. We used the same prior scales for the Bayesian Wilcoxon signed-rank test and the Bayesian RM ANOVA for the trends as described in previous sections. Bayesian Wilcoxon signed-rank tests and Bayesian RM ANOVA were computed with JASP.

Analysis of motor unit firing rate changes.

Single-target analysis. We analyzed the firing rate changes between the baseline and action phases for all four targets separately. With ΔFR_1 and ΔFR_2 referring to the changes of the firing rates of MU_1 and MU_2 between baseline and action, the following three hypotheses were considered (see Fig. 2):

H_0: no change in firing rates, i.e., $\Delta FR_1 = 0 \wedge \Delta FR_2 = 0$
H_1: successful target reach, i.e., $\Delta FR_1 > 0 \wedge \Delta FR_2 < 0$ for *T1* and *T3*, $\Delta FR_1 < 0 \wedge \Delta FR_2 > 0$ for *T2* and *T4*.
H_2: no successful target reach but a change of firing rate in at least 1 of the 2 units. This hypothesis reflects the complement of H_0 and H_1.

Bayes factors between all pairs of hypotheses were computed with the R package BFpack (42). BFpack uses default priors that do not require the specification of the scale of the expected effects (for details see Ref. 42). The analysis provides Bayes factors for all pairwise combinations of the three hypotheses, yielding in total six Bayes factors (BF_{xy} with $x \in \{0, 1, 2\}$ and $y \in \{0, 1, 2\}$ and $x \neq y$). Given that $BF_{xy} = 1/BF_{yx}$ and that $BF_{xy} = BF_{xz} \cdot BF_{zy}$, any two Bayes factors that include each hypothesis at least once contain the complete information.

The Bayes factors were interpreted as follows:

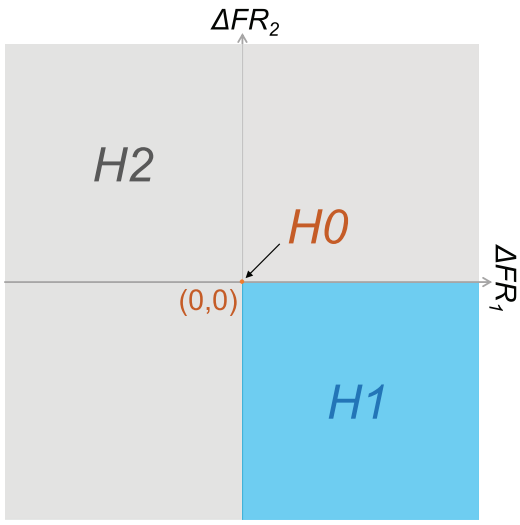


Figure 2. Illustration for 3 hypotheses used to test motor unit (MU) firing rate (FR) changes (Δ) using the target *(T)1*/*T3* area as an example. Orange color for H_0, light blue color for H_1 and gray color for H_2.

1) If the Bayes factors of one hypothesis over both of the other two hypotheses exceeded 10 (or 3), we concluded that the data provide strong (or moderate) evidence for that hypothesis. In other words, if $BF_{20} > 10$ and $BF_{21} > 10$ the data provide strong evidence for H_2. Correspondingly, if $BF_{01} > 10$ and $BF_{02} > 10$ or if $BF_{10} > 10$ and $BF_{12} > 10$ the data provide strong evidence for H_0 or H_1, respectively. For all three cases, if both BFs were larger than 3 but at least one of them was not larger than 10, we concluded that our data provide moderate evidence for H_0, H_1, or H_2, respectively.
2) In cases where no single hypothesis dominates over both of the other two hypotheses, we may still find moderate or strong evidence against H_1. If none of the conditions of *1*) applies but if either $BF_{21} > 10$ or $BF_{01} > 10$, the data provide strong evidence against H_1 regardless of the values of the other Bayes factors in each case. Likewise, if either $3 < BF_{21} \leq 10$ or $3 < BF_{01} \leq 10$, we concluded that our data provide moderate evidence against H_1.
3) If none of the conditions of *1*) or *2*) applies, the data provide only weak or anecdotal evidence with regard to H_1.

We report the Bayes factors BF_{20}, BF_{21}, and BF_{10}, from which all other Bayes factors can be computed. Although two Bayes factors would be sufficient, we report three Bayes factors for convenience. For the analyses of the population of participants, trial-averaged firing rates were used assuming statistical independence between participants. For single-participant analyses, firing rates from individual trials were used assuming statistical independence between trials.

Opposing targets analysis. We jointly analyzed the firing rate changes for pairs of opposing targets (*T1* and *T2* or *T3* and *T4*). With ΔFR_1^l and ΔFR_2^l referring to the firing rate changes of MU_1 and MU_2 for a lower target (i.e., either *T1* or *T3*) and ΔFR_1^u and ΔFR_2^u to the firing rate changes for an upper target (i.e., either *T2* or *T4*), we considered the following three hypothesis for each pair of opposing targets:

H_0: no change in firing rates for both targets, i.e., $\Delta FR_1^l = 0 \wedge \Delta FR_2^l = 0 \wedge \Delta FR_1^u = 0 \wedge \Delta FR_2^u = 0$
H_1: successful reach of both targets, i.e., $\Delta FR_1^l > 0 \wedge \Delta FR_2^l < 0 \wedge \Delta FR_1^u < 0 \wedge \Delta FR_2^u > 0$
H_2: no successful reach of both targets but a change of firing rate in at least 1 of the 2 units during at least 1 of the 2 targets. This hypothesis reflects the complement of H_0 and H_1.

The rest of this analysis was carried out in the same way as in the single-target case.

Fitting and visualizing bivariate Gaussian distributions.

When fitting bivariate Gaussian distributions to firing rates, we used the sample mean ($\hat{\mu}$) and the sample covariance matrix ($\hat{\Sigma}$). To visualize the bivariate Gaussian distributions, we used ellipses centered at $\hat{\mu}$ and with axes orientated along the eigenvectors of $\hat{\Sigma}$. The width and height of the ellipses were chosen so that a random number drawn from the bivariate Gaussian lies within the ellipse with a probability of 0.8. This was achieved by

Downloaded from journals.physiology.org/journal/jn (062.036.043.138) on June 24, 2026.

setting the width/height of the ellipse to the square roots of the eigenvalues multiplied by $2\sqrt{F^{-1}(0.8)}$ where F^{-1} is the inverse of the χ^2_k cumulative distribution function with $k = 2$ degrees of freedom (43).

RESULTS

Real-Time Displacement Control with Motor Unit Activities

Under the hypothesis of rigid control, the firing rates of any two recruited MUs would comodulate and either increase or decrease simultaneously (25). Figure 3*A* illustrates the firing rates (FRs) of a hypothetical MU pair under rigid control with firing rates confined to a one-dimensional manifold (black curve). Conversely, under the flexible control hypothesis (25), MU firing rates are not restricted to a one-dimensional manifold but instead can occupy different regions of the state space. As a consequence, firing rates can reach so-called displacement zones (25) that require opposing rate modulations from an intial set of rates (Fig. 3*A*). If participants could volitionally and consistently modulate firing rates of two MUs used for feedback to fall within the displacement zones, it would violate the rigid control hypothesis and suggest that they were able to independently control the two units and that those MUs were receiving inputs changing in opposite directions.

In the displacement control task, targets were positioned within the displacement zones. The single-session experiment included five blocks, with each block comprising 40 trials, for a total of 200 trials. Each trial consisted of two phases: the baseline phase and the action phase. A trial began with the baseline phase, during which the cursor was held over one of the two baseline areas (Fig. 3*B*, gray circles) for 3 consecutive seconds. The two baseline *areas A* and *B* corresponded to two distinct force levels. The baseline phase was followed by the action phase, where participants were required to navigate the cursor to one of the target areas *T1–T4*. *T1* or *T2* was presented after baseline *area A*, and *T3* or *T4* was presented after baseline *area B*. In each trial, only one baseline area and one target were displayed. Importantly, the target position was placed within a displacement zone relative to the average firing rates of the two MUs during the baseline phase, e.g., r_t in Fig. 3*A*. Figure 3*C* shows the cursor trajectory of an example trial.

The mean recruitment and derecruitment thresholds for the two controlled MUs were 2.1 ± 1.2% MVC (mean ± SD) and 2.7 ± 1.4% MVC for MU_1 and 2.6 ± 1.7% MVC and 2.6 ± 2.0% MVC for MU_2, respectively (Fig. 4*A*; Bayesian Wilcoxon signed-rank test $BF_{10} = 1.7$ for recruitment and $BF_{10} = 0.37$ for derecruitment thresholds). We preferentially selected MUs with low recruitment thresholds to reduce the risk of fatigue. The dorsiflexion forces exerted by the participants during the action phase remained

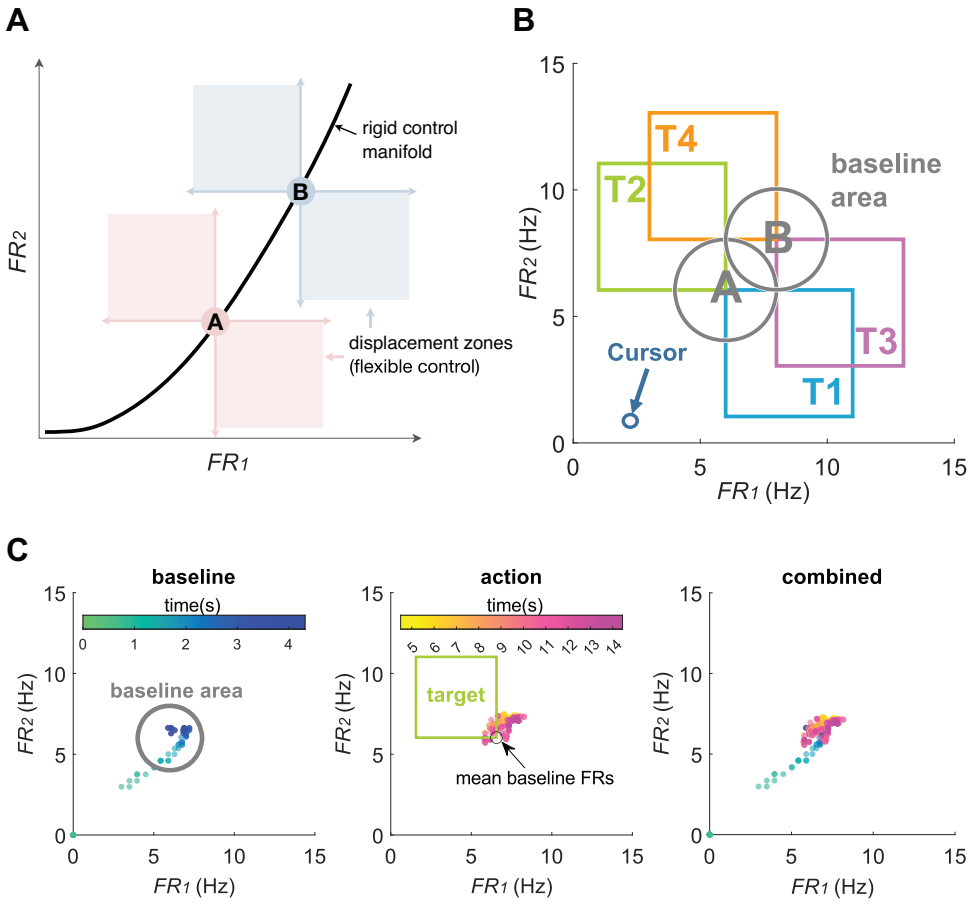


Figure 3. *A*: schematic illustration of displacement zones (red and blue) and a 1-dimensional manifold (black line) for 2 motor units (MUs) under the rigid control hypothesis. Displacement zones are defined relative to an intial set of firing rates (here, *A* and *B* as examples), requiring opposite modulation of the rates to be reached. The manifold/displacement framework follows Marshall et al. (25). FR, firing rate; r_t, firing rate at time *t*. *B*: illustration of the displacement control task. *T1–T4* refer to individual targets. *C*: cursor trajectory from an example trial. *Left*: Cursor trajectory from the beginning of the trial to the end of the 3-s holding period over the baseline area (gray). *Center*: cursor trajectory during the 10-s action phase. The targets were displayed as square boxes with a side length of 5 Hz, positioned such that their upper left vertex (for *T1* and *T3*) or lower right vertex (for *T2* and *T4*) corresponded to the averaged firing rates from the 2 MUs during the final 3 s of the baseline phase. The color depicts the time passed since the beginning of the trial. *Right*: cursor trajectory during the entire trial. The cursor position was updated every 62.5 ms. FR_1 and FR_2 correspond to the firing rates of MU_1 and MU_2, respectively. In the displacement control task, firing rates of MU_1 were mapped to cursor movement along the *x*-axis, while MU_2 was mapped to the movement along the *y*-axis.

Downloaded from journals.physiology.org/journal/jn (062.036.043.138) on June 24, 2026.

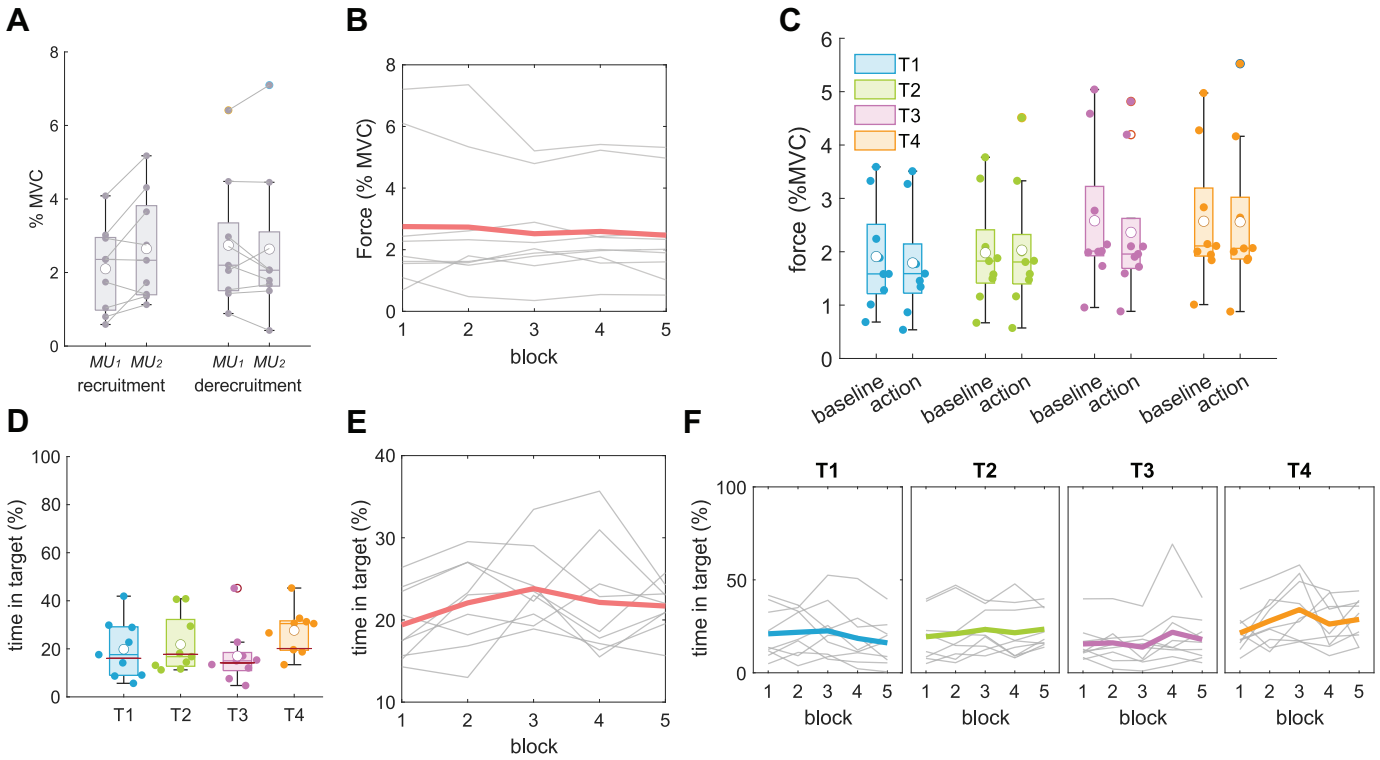


Figure 4. *A*: recruitment and derecruitment thresholds of the 2 motor units (MUs) used to control the cursor. MVC, maximum voluntary contraction. *B*: force produced across the 5 blocks during the action phase (individual participants in gray; mean across participants in red). *C*: force produced during baseline and action phases. *D*: percentage of time the cursor was held inside targets separately for each target. Horizontal dark red bars depict the chance level for each target. Chance levels were determined by randomly shuffling the targets of each target pair (*T1* and *T2*; *T3* and *T4*) and recalculating the "time in target" across the entire experiment. The random shuffling was repeated 1,000 times, and the resulting values were averaged. In *C* and *D*, each colored dot depicts 1 participant; white dots depict the mean and horizontal lines the median. *E*: percentage of time the cursor was held inside the targets across blocks for individual participants (gray) and mean across participants (red). *F*: percentage of time the cursor was held inside targets across blocks for each target. Individual participants in gray; means across participants in color.

stable across the experimental blocks (Fig. 4*B*; trend-$BF_{10} = 0.4$; see MATERIALS AND METHODS for details on trend-BF_{10}), and there was evidence for the force being dependent on the target (Fig. 4*C*; Bayesian repeated-measures ANOVA, $BF_{inclusion} > 100$, $BF_{inclusion} = 4$, and $BF_{inclusion} = 0.4$ for target, target-phase interaction, and phase, respectively). Average force levels for *T3* and *T4* were slightly higher than for *T1* and *T2*, regardless of the trial phase (see Supplemental Table S12 for results of post hoc tests).

The performance was evaluated by the percentage of time the cursor was held within the target during each trial. Overall, performance was low, with the average varying between 17% and 28% (Fig. 4*D*) across targets, and was only slightly higher than chance level (Fig. 4*D*, dark red bars). There was no evidence for a target-dependent performance (Fig. 4*D*; Bayesian repeated-measures ANOVA $BF_{inclusion}$ for target = 0.5). Furthermore, trend analysis on the slope of the performance across blocks showed no tendency of improvement in performance across blocks (Fig. 4*E*; trend-$BF_{10} = 0.6$) or target-specific learning effect (Fig. 4*F*; Bayesian repeated-measures ANOVA of trends, trend-$BF_{inclusion} = 0.9$ for target).

Restricted Modulation of Motor Unit Firing Rates in the Displacement Control Task

We compared the firing rates of both controlled MUs between baseline and action phases in the displacement control task to detect deviations from the one-dimensional manifold. During the action phase, occasional entries into the target area could occur because of random fluctuations, as also reflected in the "time in target" measurements shown in Fig. 4*D*. However, without active modulation, such entries arise solely from fluctuations, causing the cursor to drift in and out of the target area over time. Consequently, the average firing rate during the entire action phase would not exhibit any systematic modulation toward the displacement zone beyond what would be expected from statistical fluctuations.

To assess systematic firing rate modulation into the displacement zones, we calculated the average firing rates over the entire 10-s action phase and compared them statistically with the averaged firing rates across 3 s during baseline phase for each trial. Here, ΔFR_1 and ΔFR_2 are defined as

$$\Delta FR_1 = FR_1^{\text{action}} - FR_1^{\text{baseline}}$$

$$\Delta FR_2 = FR_2^{\text{action}} - FR_2^{\text{baseline}}$$

where FR_1^{action} refers to the mean firing rate during the action phase for MU_1 and FR_1^{baseline} refers to the mean firing rate during the baseline phase for MU_1. The same applies to MU_2. The following three hypotheses were evaluated with Bayesian hypothesis testing (see MATERIALS AND METHODS for details):

Downloaded from journals.physiology.org/journal/jn (062.036.043.138) on June 24, 2026.

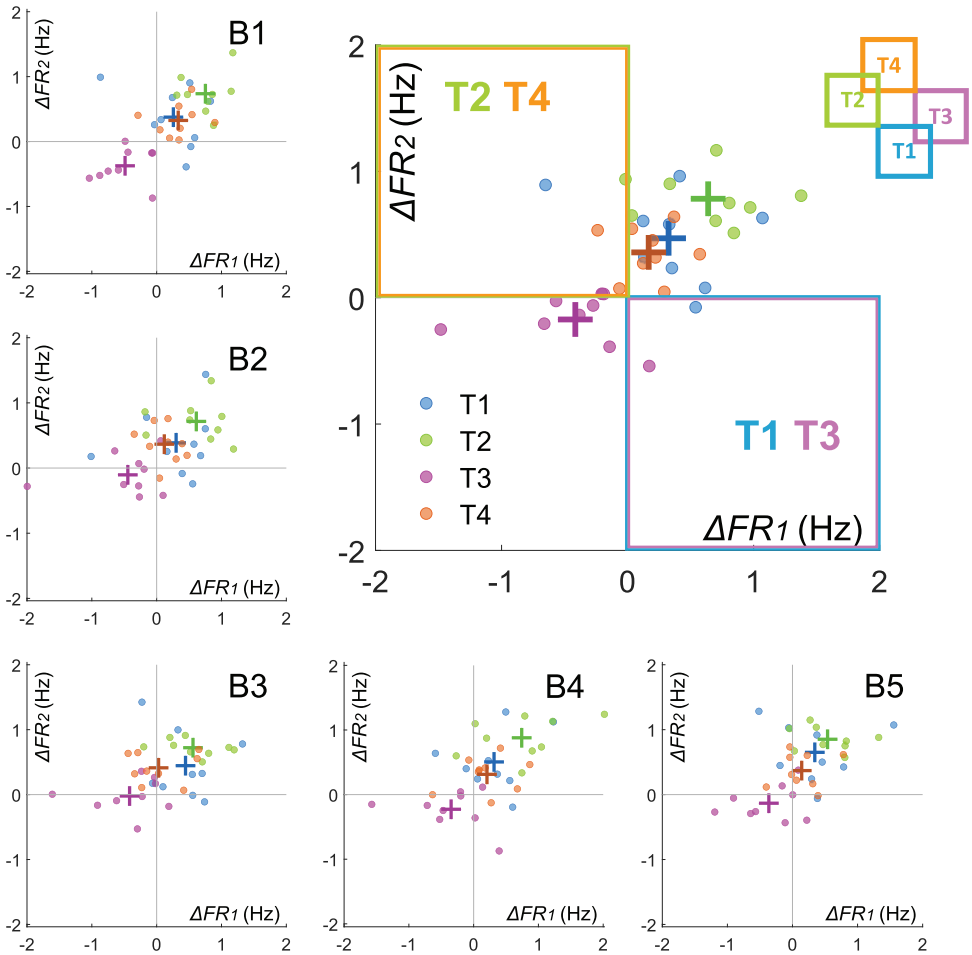


Figure 5. Averaged changes of the firing rates of motor unit (MU)$_1$ and MU_2 (ΔFR_1 and ΔFR_2) across the whole experiment (*top right*), as well as separately for *blocks 1–5* [*B1–B5*; dots: individual participants with color indicating the target (*T1–T4*); +: target-specific mean across participants]. Colored rectangular boxes label the target areas.

H_0: No change in firing rates.
H_1: Successful target reach.
H_2: Firing rate changes not in line with the target area, but at least 1 of the MUs changed its firing rate. H_2 is the complement of H_0 and H_1.

Note that unsuccessful target reach could be the result either of no firing rate modulation between action and baseline phases (hypothesis H_0) or of rate modulations outside the target areas (hypothesis H_2). By comparing the above three hypotheses using Bayes factors, we were able to distinguish between both cases.

Pooled data from all blocks and participants provided strong evidence against participants being able to modulate the FRs of the controlled MUs toward successful target reach for *T1*, *T2*, and *T3* and moderate evidence against target reach for *T4* (Fig. 5, *top right*, and Table 1). Participants did change the firing rates during action phase as compared to baseline phase ($BF_{20} > 10$ for all targets) but not toward the target area ($BF_{21} > 10$ for *T1–T3* and $BF_{21} = 7.2$ for *T4*). For the analysis of individual blocks, anecdotal evidence for successful target reach was observed only in *block 3* for *T4* (Supplemental Table S1; Fig. 5). No other blocks and targets showed evidence for successful target reach. These findings obtained from the MU firing rates were consistent with the low performance (Fig. 4*D*) and the lack of improvement in performance across blocks (Fig. 4, *E* and *F*).

Table 1. *Bayes factors quantifying relative strength of evidence for H_0, H_1, and H_2 separately for targets T1–T4*

	BF_{20}	BF_{21}	BF_{10}
T1	243	124	2
T2	2.8×10^5	142	1,980
T3	28	18	1.5
T4	259	7.2	36

BF, Bayes factor. See MATERIALS AND METHODS.

We assessed the variability of firing rate differences between baseline and action phases for each individual participant (Fig. 6, *A* and *B*). Firing rate variability was quantified using the standard deviation of ΔFRdiff and ΔFRsum, defined as follows:

$$\Delta FR\text{diff} = \Delta FR_1 - \Delta FR_2$$

$$\Delta FR\text{sum} = \Delta FR_1 + \Delta FR_2$$

The standard deviation of ΔFRsum captures the variability in the firing rates of the two MUs along the diagonal from the origin toward the upper right in the state space (Fig. 6*A*) and is expected to correlate with the variability of the exerted force, whereas the standard deviation of ΔFRdiff quantifies variability in firing rates perpendicular to this diagonal. There was no indication that either of these variabilities changed across blocks (Fig. 6, *C* and *D*, trend-$BF_{10} = 0.4$ and 0.3 for *C* and *D*, respectively) or in a target-specific way (Fig. 6, *E* and *F*,

Downloaded from journals.physiology.org/journal/jn (062.036.043.138) on June 24, 2026.

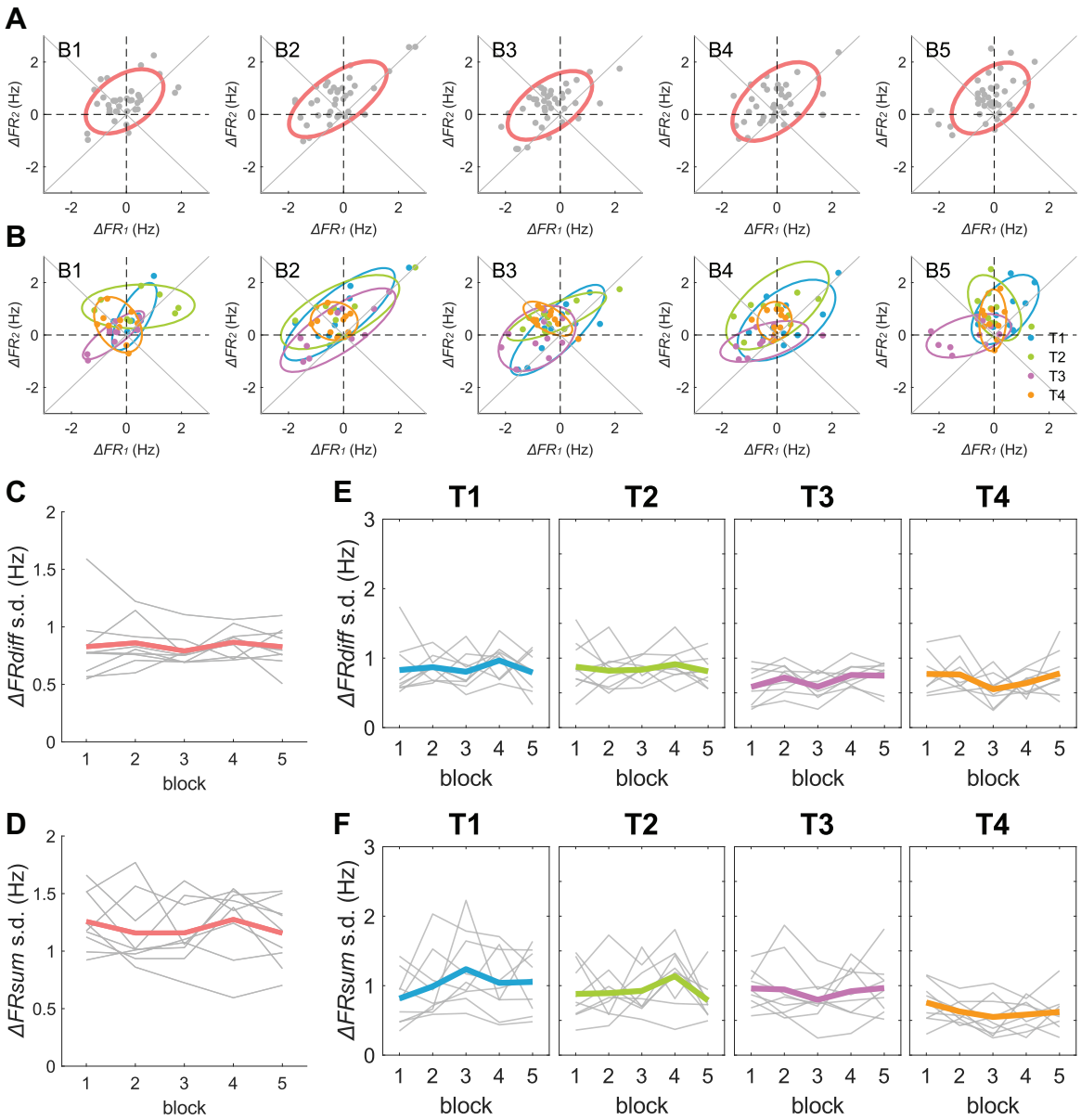


Figure 6. *A* and *B*: distribution of changes of the firing rates of motor unit (MU)$_1$ and MU_2 (ΔFR_1 and ΔFR_2) from a single participant across blocks. Data pooled across all targets (*A*; gray dots: single trials) and separately for each target across blocks (*B*). Ellipses visualize bivariate Gaussian distributions fitted to firing rate differences, with contour lines containing 80% of the data probability. *B1–B5*, *blocks 1–5*. *C* and *D*: SD of the difference (*C*) and the sum (*D*) of ΔFR_1 and ΔFR_2 (individual participants in gray; mean across participants in red). *E* and *F*: same as *C* and *D* but separately for targets *T1–T4*.

Bayesian repeated-measures ANOVA of trends, trend-$BF_{inclusion}$ for target = 0.6 and 0.7 for *E* and *F*, respectively).

We further analyzed target reach in individual participants in the displacement control task. Four out of 10 participants (including the 1 participant excluded from the preceding population analysis, *P28*) showed moderate to strong evidence for target reach for one or two targets (Fig. 7*A*). Figure 7*B* shows the ΔFR_1 and ΔFR_2 for each individual trial across the four targets for a single participant (*P23*), who demonstrated evidence for target reach for *T2* and *T4* but not for *T1* and *T3*. Note that *T1* and *T3* belong to one quadrant, whereas *T2* and *T4* belong to a different, but also shared, quadrant. Such single-quadrant target reaching was observed in all four participants who successfully reached individual targets. Although four participants demonstrated successful reach of individual targets, none was able to reach opposing targets corresponding to the same baseline area, such as *T1* and *T2* or *T3* and *T4*. This result suggests that successful target reach was unlikely achieved through flexible MU control, as participants would likely have been able to navigate the cursor also to targets in the opposite quadrant if such control had been present.

To test on the population level whether there was evidence for successful target reach to targets in opposite quadrants, we modified the test hypotheses from the previous section. H_1 now considers both opposing targets:

H_0: No change in firing rates.
H_1: Successful target reach for targets in opposite quadrants, i.e., either *T1* and *T2* or *T3* and *T4*.

Downloaded from journals.physiology.org/journal/jn (062.036.043.138) on June 24, 2026.

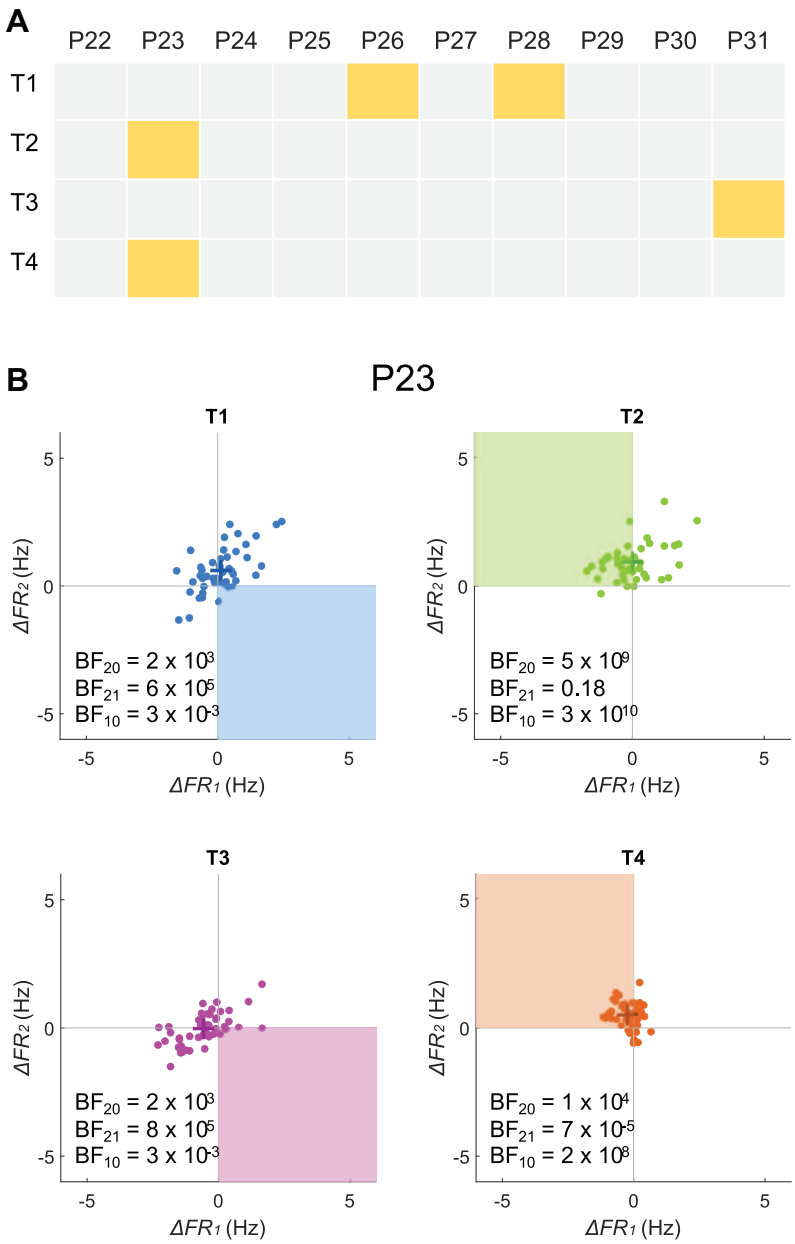


Figure 7. *A*: distribution of successful target reach for each participant (*P22–P31*). Cases with moderate or strong evidence in favor of successful target reach are marked in yellow. Bayes factors (BFs) can be found in Supplemental Table S2. *T1–T4*, *targets 1–4*. *B*: changes of the firing rates of motor unit (MU)$_1$ and MU_2 (ΔFR_1 and ΔFR_2) across the whole experiment separated by targets for 1 participant (*P23*; dots: individual trials; +: mean across all trials from the target). Colored rectangular areas label the target zones for the individual target.

H_2: Firing rate changes not in line with the target area, but at least 1 of the units changed its firing rate. H_2 is the complement of H_0 and H_1.

On the population level, our results provide strong evidence against successful reach of opposing targets ($BF_{21} > 10$ and $BF_{20} > 10$ for both *T1* and *T2* and *T3* and *T4*) (Table 2).

Table 2. *Bayes factors quantifying relative strength of evidence for H_0, H_1, and H_2 for targets from opposing quadrants*

	BF_{20}	BF_{21}	BF_{10}
T1 and *T2*	5.9×10^5	1.9×10^3	304
T3 and *T4*	1.3×10^5	63	2×10^3

BF, Bayes factor; *T1–T4*, *targets 1–4*.

No Systematic Evidence for Displacement was Observed under Less Constrained Control Conditions

In a second experiment, referred to here as the difference control task, we investigated whether participants could modulate firing rates of pairs of MUs violating rigid control under a less restrictive control condition. In this task, the vertical cursor position was controlled by the sum of the firing rates of two MUs, while the horizontal cursor velocity was controlled by the difference of their firing rates. In this task, the targets were placed at both ends of the horizontal axis (Fig. 8*A*). Since participants only had to generate differences in the firing rates to reach the targets, the areas in the state space relevant to successful target reach included the respective halves of the state space (Fig. 8*B*). These areas included the displacement zones described in the previous section, as well as areas outside the displacement zones, as

Downloaded from journals.physiology.org/journal/jn (062.036.043.138) on June 24, 2026.

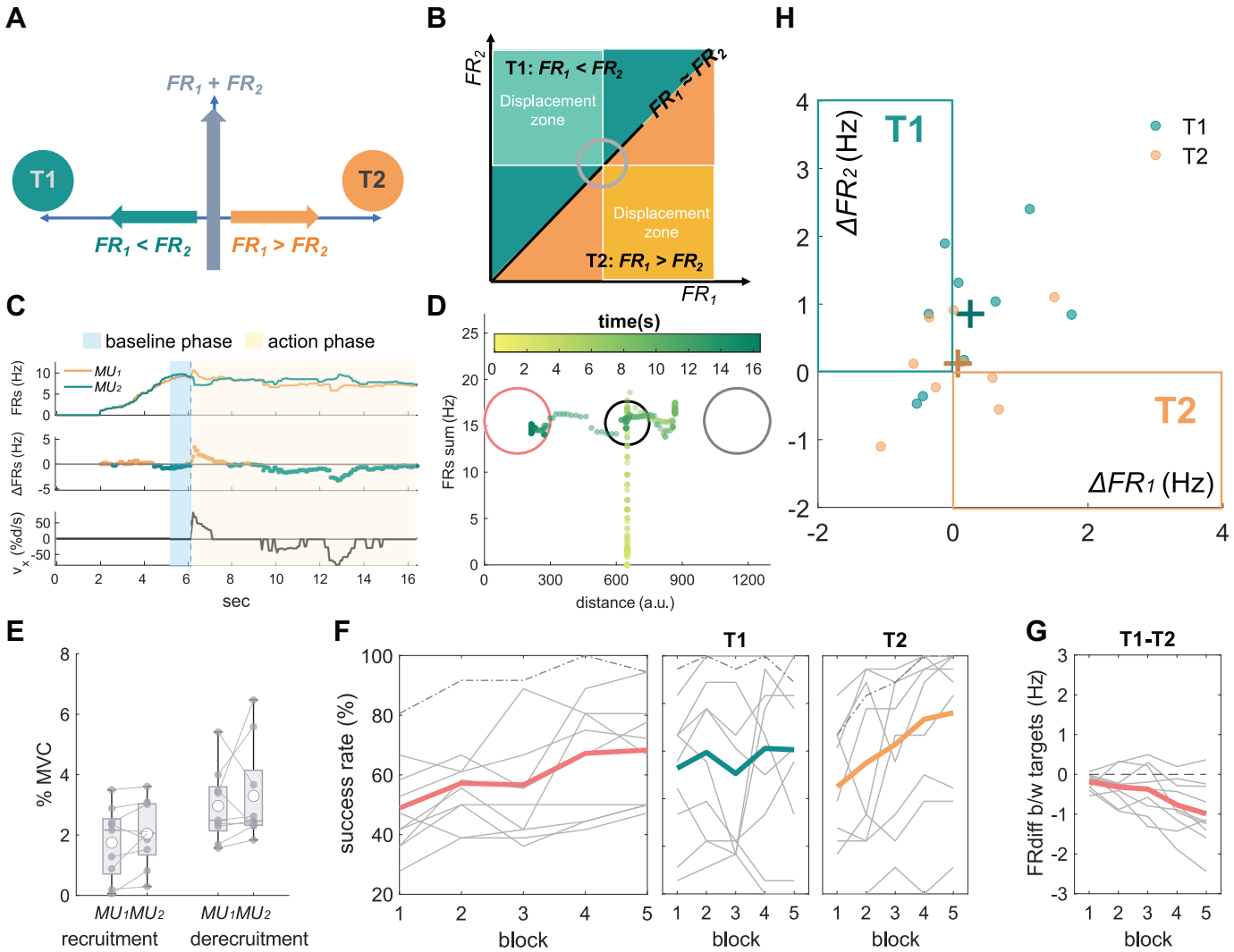


Figure 8. *A*: illustration of the control scheme in the difference control task. The cursor position along the vertical axis was controlled by the sum of the firing rates of the 2 motor units (MUs), and the cursor velocity along the horizontal axis was controlled by the difference between their firing rates (FRs). *B*: illustration of firing rate areas in the state space relevant for target reach. Each area is subdivided into regions within and outside the displacement zone. The baseline area is depicted by the gray circle. *C* and *D*: firing rates of the 2 MUs (FR_1 and FR_2), horizontal velocity (*D*), and cursor trajectory (*D*) from an example trial. *C*, *middle*: Δ*FR*s refers to the difference between FR_1 and FR_2, with color coding indicating which MU exhibits a higher firing rate. *C*, *bottom*: velocity of the cursor movement (v_x) in percentage of the total distance from the baseline area to the target per second. *D*: the black circle indicates the baseline area. The red circle represents the active target, and the gray circle represents the inactive target. a.u., Arbitrary units. *E*: recruitment and derecruitment thresholds of the 2 MUs used to control the cursor. MVC, maximum voluntary contraction. *F*: success rate across the 5 control blocks. *Left*: combined *target* (*T*)*1* and *T2*; *center* and *right*: separated for *T1* and *T2* (individual participants in gray; mean across participants in color). The data for the single participant whose neural data was excluded (see MATERIALS AND METHODS) are represented by a dash-dot line. *G*: firing rate differences between the targets across 5 blocks during the action phase. *FR*diff b/w targets (with b/w denoting "between") here refers to $(FR_1^{T1} - FR_2^{T1}) - (FR_1^{T2} - FR_2^{T2})$ during the action phase, where FR_1^{T1} and FR_2^{T1} refer to averaged firing rates of MU_1 and MU_2, respectively, in trials with *T1* (the same applies to *T2* trials). *H*: mean ΔFR_1 and ΔFR_2 for individual participants (dots) and mean across participants (crosses). Mean ΔFR_1 and ΔFR_2, similar to the displacement task, were defined as the average firing rate differences between the action phase and the baseline phase. Colored rectangular boxes label the displacement zones for the 2 targets.

illustrated in Fig. 8*B*. A threshold on the firing rate differences was applied, below which the horizontal velocity was set to zero (see MATERIALS AND METHODS for details). Participants first moved the cursor into the baseline area and held it there for 1 consecutive second (baseline phase), with the horizontal position fixed. After this baseline phase, the trial proceeded to the action phase, during which the cursor could move freely horizontally and vertically. A trial was considered successful if a participant could hold the cursor at the target for 3 consecutive seconds. Otherwise, the trial failed with a timeout after 30 s. The single-session task consisted of five blocks, with a total of 180 trials. Figure 8, *C* and *D*, show the firing rates of the two controlled MUs and the cursor trajectory over time from an example trial.

The mean recruitment and derecruitment thresholds were 1.7 ± 1.2% MVC and 3.0 ± 1.2% MVC for MU_1 and 2.0 ± 1.1% MVC and 3.3 ± 1.6% MVC for MU_2 (Fig. 8*E*; Bayesian Wilcoxon signed-rank test $BF_{10} = 1.98$ for recruitment and $BF_{10} = 0.51$ for derecruitment thresholds). The results showed that participants modulated firing rate differences,

Downloaded from journals.physiology.org/journal/jn (062.036.043.138) on June 24, 2026.

Table 3. *Bayes factors quantifying relative strength of evidence for H_0, H_1, and H_2 in the difference control experiment*

	BF_{20}	BF_{21}	BF_{10}
T1	2.6	0.9	2.8
T2	0.18	1.4	0.1

Same hypotheses as in Table 1. The data provide inconclusive evidence for *target 1* (*T1*) and strong evidence for H_0 for *target 2* (*T2*), i.e., no evidence for flexible motor unit (MU) control. BF, Bayes factor.

and this modulation increased across blocks in line with the increased performance (Fig. 8, *F* and *G*; Fig. 8*F*, *left*: trend-$BF_{10} > 100$, Fig. 8*F*, *center* and *right*: trend-$BF_{10} = 0.3$ and 360 for *T1* and *T2*, Fig. 8*G*: trend-$BF_{10} = 40$; Supplemental Figs. S1 and S2a). The observed firing rate differences, however, do not necessarily imply deviations from the one-dimensional manifold (Fig. 3*A*), as these differences could be within or outside of the displacement zones (Fig. 8*B*). To clarify this point, we conducted an analysis comparing the firing rate changes between the baseline and action phases, using the same three hypothesis tests as in the displacement control task.

There was no evidence for firing rate modulation toward the displacement zones of the corresponding targets for data aggregated across blocks (Fig. 8*H* and Table 3), in line with results from the analysis of individual blocks (see Supplemental Fig. S3 and Supplemental Table S3). Furthermore, there was strong evidence against successful target reach to both opposing targets (Table 4). Taken together, these results suggest that participants were able to learn the task under less strict control conditions. Moreover, participants improved performance within a single-session training by increasing the difference in firing rates between the two MUs across blocks. However, the firing rate differences were not produced by modulating the firing rates of the MUs into the corresponding displacement zones.

DISCUSSION

Lack of Flexibility in MU Control

The possibility of flexible MU control remains debated because of contradictory findings regarding the selective recruitment of MUs, and little is known about whether individuals can modulate the activity of two MUs independently. In this study, we investigated whether the activity of two MUs from the same pool can be voluntarily modulated in a way that the firing rate is increased in one unit and decreased in the other. Demonstrating this capability would provide compelling evidence for the human ability to selectively control individual MUs within a pool of a single muscle. We focused solely on flexible firing rate control without allowing for recruitment/derecruitment strategies and employed two tasks with different degrees of motor constraints. On the population level, our results from a group of participants revealed no evidence that MU firing rates could deviate from rigid control. Nevertheless, individual participant analysis showed that 4 out of 10 participants in the displacement control task demonstrated moderate to strong evidence of successful individual target reach. However, it is important to note that no participant was able to reach opposing targets. When two targets were reached, they were located within the same quadrant relative to the baseline area. The inability to reach opposing targets suggests a lack of flexible MU control, as participants should have been able to voluntarily navigate the cursor to both opposing targets if MUs were flexibly controlled by independent inputs. Instead, target reach appeared to be affected by factors that consistently drove the firing rates toward the same quadrant. This outcome may be attributed to intrinsic properties of MUs in their response to synaptic inputs, such as the influence of persistent inward currents (PICs). One effect of PICs is the hysteresis in firing rates when MUs receive a triangular pattern of increasing and decreasing input (44). When the two controlled MUs exhibit different ascending and descending slopes in their firing rate hysteresis, it can result in a positional shift from the baseline. By first increasing and then decreasing the exerted force, participants could have potentially guided the cursor into the target area as illustrated in Fig. 9. Depending on the relative slopes of the two MUs, participants could have reached either *T1* and *T3* or *T2* and *T4* in the displacement control task with subtle force variations. However, such a control strategy would not allow the reaching of opposing targets, which aligns with our observations. Therefore, we believe that the individual target reach was not the result of flexible MU control and conclude that flexible MU control in the human tibialis anterior muscle was not achieved within a single day of neurofeedback training in our experiments.

We did not identify the exact mechanism by which some participants were able to reach individual targets. We consider it plausible that participants exploited the firing rate hysteresis resulting from PICs (Fig. 9), which is also consistent with the observation that none of our participants was able to reach opposing targets. However, we did not provide direct experimental evidence for this hypothesis as we cannot measure PICs and our force measurements were of limited precision that may not be sufficient to reliably detect relatively subtle modulations.

Some studies have demonstrated the selective activation of MUs from the human tibialis anterior (28, 30) and the biceps brachii (32) muscles. However, showing single MU activation without showing the reversal of the recruitment order cannot be considered an indication of flexible control as it may be due to the derecruitment of the other MUs (26). Additionally, results derived from multicompartment muscles should be interpreted with caution, as MUs from different muscle compartments that can receive independent input might be involved (45). Although reversing MU recruitment order has been reported during fast force contractions in the human tibialis anterior muscle (29), the

Table 4. *Bayes factors quantifying relative strength of evidence for H_0, H_1, and H_2 for trials from opposing targets*

	BF_{20}	BF_{21}	BF_{10}
T1 and *T2*	29.1	129.6	0.23

Same hypotheses as in Table 2. BF, Bayes factor; *T1* and *T2*, *targets 1* and *2*.

Downloaded from journals.physiology.org/journal/jn (062.036.043.138) on June 24, 2026.

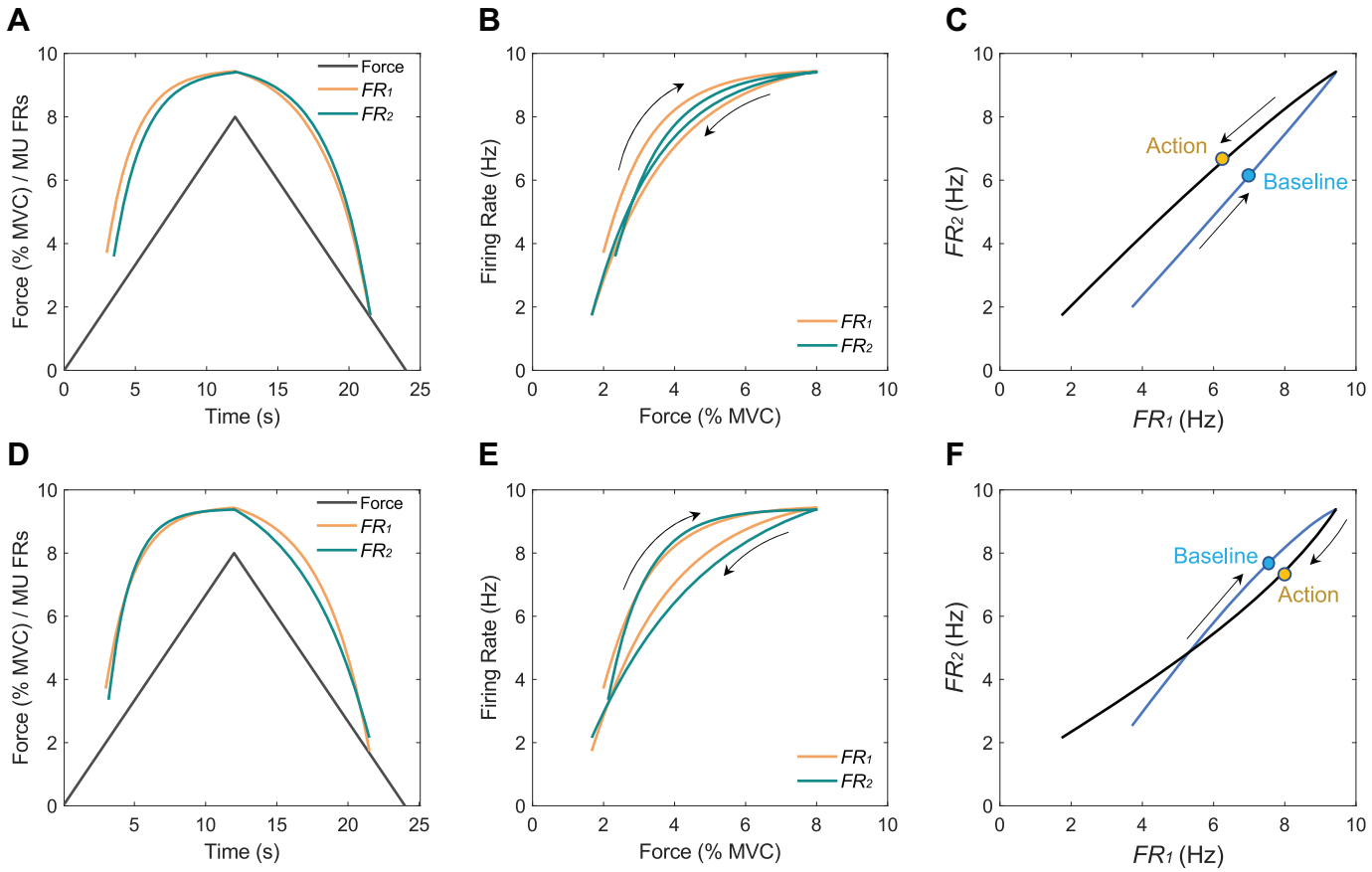


Figure 9. Illustration of how single-quadrant target reach could be achieved because of hysteresis from persistent inward currents. *A–C*: development of time vs. force [% maximum voluntary contraction (MVC)] and motor unit (MU) firing rates (*FR*s) (*A*), force vs. MU firing rates (*B*), and the firing rates in the state space (*C*) from a pair of MUs. In this scenario, if participants increase and then decrease force, it would be possible to reach targets in the upper left quadrant, such as *T2* and *T4*, in the displacement control task but not *T1* or *T3*. Blue line: force ramp-up. Black line: force ramp-down. *D–F*: similar to *A–C*. With MU hysteresis properties as illustrated, participants would be able to reach targets in the lower right quadrant, such as *T1* and *T3*, in the displacement control task but not *T2* or *T4*. The arrows indicate the direction of the firing rate changes over time.

findings have not been consistent across different muscles (13, 14, 46, 47). A recent study by Marshall et al. (25) demonstrated that the activities of MUs can deviate from a one-dimensional manifold during force modulation and also as a result of electrical stimulation of neighboring cortical sites. These findings suggest that direct cortical control over MUs is implemented in the motor system and that flexible MU control is a normal feature of skilled performance. It is therefore plausible to anticipate that participants can readily utilize this flexibility when given direct visual feedback of MU activities. However, our findings suggest that participants did not easily use this flexibility, at least not within a single training session.

The failure to identify flexibility in this study is unlikely attributable to the usage of sEMG recordings rather than intramuscular recordings, as the two methods show a high level of agreement, with $>$ 80% of action potentials identified in common (48–50). Yet the selection of the test muscle may be a contributing factor. Like upper limb muscles, motoneurons in the human tibialis anterior muscle receive fast-conducting monosynaptic corticomotoneuronal (CM) connections (51, 52), suggesting potential for direct cortical control. However, the CM connectivity patterns between upper motoneurons and spinal motoneurons may differ between upper and lower limbs. The absence of robust MU firing rate modulation in the displacement zone of our experiments may be due to our focus on activated MUs (excluding any effects from recruitment and derecruitment) and that participants were requested to perform tasks where trials lasted over seconds. In contrast, Marshall et al. (25) showed that deviations from rigid control could be observed when comparing MU activity during force modulations at varying speeds including rapid force offsets, such as in sinusoidal movements at different frequencies where a fast force offset was required to track the given force profile. Since our experiment specifically instructed participants to keep the controlled MUs active, fast force offsets were discouraged. However, if flexible control is indeed a normal feature of motor control, participants should be able to naturally utilize the flexibility to reach the targets in displacement zones without the need for excessive training and regardless of the required force modulation. It remains unclear why the flexibility observed in macaque upper limb muscles does not extend to the modulation of MU firing rates in the human tibialis anterior muscle. Could the distinct activity patterns observed across different force profiles be governed by motor programs associated with each force profile, potentially representing the most optimal strategy for motor unit control?

Downloaded from journals.physiology.org/journal/jn (062.036.043.138) on June 24, 2026.

If this is the case, the observations reported in Marshall et al. (25) may reflect learned responses tailored to specific motor tasks rather than presence of readily available flexible MU control, where firing rates can be adjusted quickly and freely. Further research is required to address these unresolved questions.

When executing movement tasks, muscle groups involved in the same task work together as a synergy to increase the efficiency (53). A similar concept may apply to motoneurons, where motoneuron synergies refer to functional groups of motor units from one or more muscles (18, 19, 54, 55). The observed changes in recruitment order across different tasks involving the same muscle suggest that flexible MU activation is associated with the engagement of distinct synergy groups (54). In this study, we found no evidence that participants could independently modulate the firing rates of MUs within the same muscle, despite potential behavioral changes such as small ankle rotations. This may be attributed to the fact that the majority of MUs in the tibialis anterior muscle likely belong to the same MU synergy group (20, 55). In the study by Rossato et al. (27), which employed an experimental paradigm similar to but distinct from ours, using a less stringent condition without the constraints on derecruitment and with a target area extending beyond the displacement zones participants were also unable to volitionally dissociate activities of a MU pair from either the same muscle or synergistic muscles during online feedback control. Future research may investigate whether flexible control over MUs from a single muscle, but belonging to distinct motor unit synergies, can be achieved through neurofeedback.

Limitations

The selection of MUs might have influenced the observed properties of the MUs: First, one criterion during MUs selection was to select MUs with similar recruitment thresholds (Supplemental Fig. S4) to ensure that the firing rate of the lower recruitment threshold unit did not reach saturation when the other one was recruited. However, MUs with similar recruitment thresholds are more synchronized when firing at similar frequencies (56), implying that these MUs may receive a larger proportion of common input compared to independent input (23). Second, the controlled MUs exhibited a limited range of firing rate variation of $<$2 Hz (Fig. 6), which may have been the result of MU selection. We selected MUs with low recruitment thresholds in particular so that the training time could be extended and the risk of fatigue was minimized. This may have led to reduced operational range of MU firing rates, as low recruitment threshold units ($<$10% MVC) typically exhibit an initial acceleration in firing rates upon recruitment, followed by a narrow rate modulation before reaching saturation (57, 58). This nonlinear acceleration of firing rates is attributed to the amplification of synaptic input through the activation of PICs at or below the recruitment threshold, a phenomenon more pronounced in MUs with lower recruitment thresholds (59, 60). PICs not only limit the efficacy of additional input once they are activated (44, 61) but also enable motoneurons to generate sustained repetitive firing even after the cessation of the synaptic input (62). These effects can cause the firing rates of MUs with low recruitment thresholds to be less reflective of the actual synaptic input. On the other hand, MUs with higher recruitment thresholds have a more linear force-firing rate relationship (63). Using MUs with higher recruitment thresholds may offer a larger range for firing rate modulation and reduced synchronization, but it comes with the trade-off of increased likelihood of fatigue, potentially limiting the amount of available training time within a session.

A study in nonhuman primates suggested multiple cortical drives enabling flexible control of MUs (25). However, it does not clarify whether these connections can be selectively and voluntarily controlled. In our study, we did not observe volitional control of MU activities that violates the rigid control strategy within single-session training in both tasks. The findings from the difference control task further suggest that violation of a rigid control strategy is not easy to achieve; otherwise, it would likely have been the preferred approach employed by the participants. Even though the displacement control task could not be accomplished within a single-session training, it is still possible that such a control skill could be acquired over an extended period of practice. Studies have shown that 1 day of training was insufficient for learning a novel activity pattern that falls outside the original manifold of the motor cortex (64), but the learning could occur over multiple days (65). Similarly, adapting to an entirely new muscle synergy after a remapping of muscle activation patterns did not occur within a single day (66) but was achievable with multiday training (67). Although it remains unclear whether long-term skill acquisition, such as in musicians, leads to greater flexibility in individual MUs, these individuals have been shown to exhibit greater motor-cortical excitability and plasticity compared to untrained individuals (68, 69). Technical challenges remain in conducting such an experiment over multiple days because of the difficulty of consistently tracking the same MUs across days (70), and learning might not transfer to another day when the selected MUs are varying. Improvements in cross-day MU tracking methodologies could enable future experiments addressing these questions.

DATA AVAILABILITY

Data availability for reasonable requests will be subject to applicable data protection requirements.

SUPPLEMENTAL MATERIAL

Supplemental Figs. S1–S40 and Supplemental Tables S1–S12: https://doi.org/10.5281/zenodo.17943366.

ACKNOWLEDGMENTS

We thank Deren Yusuf Barsakcioglu for assistance with the decomposition algorithm and Tobias Pistohl for assistance in resolving various technical challenges. We thank Hüseyin Cardakkaya for creating the illustration in Fig. 1.

During the preparation of this manuscript, the authors used ChatGPT to improve the language and readability of the text. The manuscript was written by the authors, who reviewed and approved all revisions and take full responsibility for the final published version.

Preprint is available at https://www.biorxiv.org/content/10.1101/2025.02.10.637074v1.

Downloaded from journals.physiology.org/journal/jn (062.036.043.138) on June 24, 2026.

GRANTS

This research was supported in part by the European Commission Grant H2020 NIMA (FETOPEN 899626), European Research Council (ERC) under the Synergy Grant Natural BionicS (810346), the EPSRC Transformative Healthcare for 2050 project NISNEM Technology (EP/T020970/1), the German Research Foundation (DFG) through Grant No. INST 39/1014-1, the state of Baden-Württemberg through the Struktur- und Innovationsfonds (SI-BW). J.I. was supported by an ERC Starting Grant (101077693) and in part by a Consolidación Investigadora grant (CNS2022-135366) funded by MCIN/AEI/10.13039/501100011033 and UE's NextGenerationEU/PRTR funds.

DISCLOSURES

D.F. is inventor of two patents (Neural Interface, UK Patent Application No. GB1813762.0. August 23, 2018 and Neural Interface, UK Patent Application No. GB2014671.8. September 17, 2020) related to the methods and applications of this work. J.I. is inventor of a patent (UK Patent Application No. GB2014671.8. September 17, 2020). D.F. is also Scientific Advisor for neural interfacing for Meta and Reality Labs and for high-density EMG technology for OT Bioelettronica, Italy. None of the other authors has any conflicts of interest, financial or otherwise, to disclose.

AUTHOR CONTRIBUTIONS

M.-J.L., P.O., D.F., and C.M. conceived and designed research; M.-J.L. performed experiments; M.-J.L. and C.M. analyzed data; M.-J.L., P.O., H.-Y.H., J.M., J.I., D.F., and C.M. interpreted results of experiments; M.-J.L. prepared figures; M.-J.L. and C.M. drafted manuscript; M.-J.L., P.O., H.-Y.H., J.M., J.I., D.F., and C.M. edited and revised manuscript; M.-J.L., P.O., H.-Y.H., J.M., J.I., D.F., and C.M. approved final version of manuscript.

REFERENCES

1. **Heckman CJ**, **Enoka RM.** Motor unit. *Compr Physiol* 2: 2629–2682, 2012. doi:10.1002/j.2040-4603.2012.tb00465.x.
2. **Eden J**, **Bräcklein M**, **Ibáñez J**, **Barsakcioglu DY**, **Di Pino G**, **Farina D**, **Burdet E**, **Mehring C.** Principles of human movement augmentation and the challenges in making it a reality. *Nat Commun* 13: 1345, 2022. doi:10.1038/s41467-022-28725-7.
3. **Holobar A**, **Farina D.** Noninvasive neural interfacing with wearable muscle sensors: combining convolutive blind source separation methods and deep learning techniques for neural decoding. *IEEE Signal Process Mag* 38: 103–118, 2021. doi:10.1109/MSP.2021.3057051.
4. **Barsakcioglu DY**, **Bracklein M**, **Holobar A**, **Farina D.** Control of spinal motoneurons by feedback from a non-invasive real-time interface. *IEEE Trans Biomed Eng* 68: 926–935, 2021. doi:10.1109/TBME.2020.3001942.
5. **Bräcklein M**, **Ibáñez J**, **Barsakcioglu DY**, **Farina D.** Towards human motor augmentation by voluntary decoupling beta activity in the neural drive to muscle and force production. *J Neural Eng* 18, 2021. doi:10.1088/1741-2552/abcdbf.
6. **Rossato J**, **Hug F**, **Tucker K**, **Gibbs C**, **Lacourpaille L**, **Farina D**, **Avrillon S.** I-Spin live, an open-source software based on blind-source separation for real-time decoding of motor unit activity in humans. *eLife* 12: RP88670, 2024. doi:10.7554/eLife.88670.3.
7. **Senn W**, **Wyler K**, **Clamann HP**, **Kleinle J**, **Lüscher HR**, **Müller L.** Size principle and information theory. *Biol Cybern* 76: 11–22, 1997. doi:10.1007/s004220050317.
8. **d'Avella A**, **Portone A**, **Fernandez L**, **Lacquaniti F.** Control of fast-reaching movements by muscle synergy combinations. *J Neurosci* 26: 7791–7810, 2006. doi:10.1523/JNEUROSCI.0830-06.2006.
9. **Bernstein NA.** *On the Construction of Movements*. Medgiz, 1947.
10. **Milner-Brown HS**, **Stein RB**, **Yemm R.** The orderly recruitment of human motor units during voluntary isometric contractions. *J Physiol* 230: 359–370, 1973. doi:10.1113/jphysiol.1973.sp010192.
11. **Henneman E.** Relation between size of neurons and their susceptibility to discharge. *Science* 126: 1345–1347, 1957. doi:10.1126/science.126.3287.1345.
12. **Henneman E**, **Clamann HP**, **Gillies JD**, **Skinner RD.** Rank order of motoneurons within a pool: law of combination. *J Neurophysiol* 37: 1338–1349, 1974. doi:10.1152/jn.1974.37.6.1338.
13. **Desmedt JE**, **Godaux E.** Fast motor units are not preferentially activated in rapid voluntary contractions in man. *Nature* 267: 717–719, 1977. doi:10.1038/267717a0.
14. **Desmedt JE**, **Godaux E.** Ballistic contractions in man: characteristic recruitment pattern of single motor units of the tibialis anterior muscle. *J Physiol* 264: 673–693, 1977. doi:10.1113/jphysiol.1977.sp011689.
15. **Riek S**, **Bawa P.** Recruitment of motor units in human forearm extensors. *J Neurophysiol* 68: 100–108, 1992. doi:10.1152/jn.1992.68.1.100.
16. **Thomas CK**, **Ross BH**, **Stein RB.** Motor-unit recruitment in human first dorsal interosseous muscle for static contractions in three different directions. *J Neurophysiol* 55: 1017–1029, 1986. doi:10.1152/jn.1986.55.5.1017.
17. **Feiereisen P**, **Duchateau J**, **Hainaut K.** Motor unit recruitment order during voluntary and electrically induced contractions in the tibialis anterior. *Exp Brain Res* 114: 117–123, 1997. doi:10.1007/PL00005610.
18. **Hug F**, **Avrillon S**, **Ibáñez J**, **Farina D.** Common synaptic input, synergies and size principle: Control of spinal motor neurons for movement generation. *J Physiol* 601: 11–20, 2023. doi:10.1113/JP283698.
19. **Hug F**, **Avrillon S**, **Sarcher A**, **Del Vecchio A**, **Farina D.** Correlation networks of spinal motor neurons that innervate lower limb muscles during a multi-joint isometric task. *J Physiol* 601: 3201–3219, 2023. doi:10.1113/JP283040.
20. **DelVecchio A**, **Germer C**, **Kinfe TM**, **Nuccio S**, **Hug F**, **Eskofier B**, **Farina D**, **Enoka RM.** Common synaptic inputs are not distributed homogeneously among the motor neurons that innervate synergistic muscles (Preprint). *BioRxiv* 2022.01.23.477379, 2022. doi:10.1101/2022.01.23.477379.
21. **Farina D**, **Negro F**, **Dideriksen JL.** The effective neural drive to muscles is the common synaptic input to motor neurons. *J Physiol* 592: 3427–3441, 2014. doi:10.1113/jphysiol.2014.273581.
22. **Farina D**, **Negro F.** Common synaptic input to motor neurons, motor unit synchronization, and force control. *Exerc Sport Sci Rev* 43: 23–33, 2015. doi:10.1249/JES.0000000000000032.
23. **Negro F**, **Yavuz U**, **Farina D.** The human motor neuron pools receive a dominant slow-varying common synaptic input. *J Physiol* 594: 5491–5505, 2016. doi:10.1113/JP271748.
24. **De Luca CJ**, **Erim Z.** Common drive of motor units in regulation of muscle force. *Trends Neurosci* 17: 299–305, 1994. doi:10.1016/0166-2236(94)90064-7.
25. **Marshall NJ**, **Glaser JI**, **Trautmann EM**, **Amematsro EA**, **Perkins SM**, **Shadlen MN**, **Abbott LF**, **Cunningham JP**, **Churchland MM.** Flexible neural control of motor units. *Nat Neurosci* 25: 1492–1504, 2022. doi:10.1038/s41593-022-01165-8.
26. **Bräcklein M**, **Barsakcioglu DY**, **Ibáñez J**, **Eden J**, **Burdet E**, **Mehring C**, **Farina D.** The control and training of single motor units in isometric tasks are constrained by a common input signal. *eLife* 11: e72871, 2022. doi:10.7554/eLife.72871.
27. **Rossato J**, **Avrillon S**, **Tucker K**, **Farina D**, **Hug F.** The volitional control of individual motor units is constrained within low-dimensional neural manifolds by common inputs. *J Neurosci* 44: e0702242024, 2024. doi:10.1523/JNEUROSCI.0702-24.2024.
28. **Hodson-Tole EF**, **Wakeling JM.** Motor unit recruitment for dynamic tasks: current understanding and future directions. *J Comp Physiol B* 179: 57–66, 2009. doi:10.1007/s00360-008-0289-1.
29. **Grimby L**, **Hannerz J.** Tonic and phasic recruitment order of motor units in man under normal and pathological conditions. In: *Human Reflexes, Pathophysiology of Motor Systems, Methodology of Human Reflexes*. Karger Publishers, 225–233, 1973.
30. **Harrison VF**, **Mortensen OA.** Identification and voluntary control of single motor unit activity in the tibialis anterior muscle. *Anat Rec* 144: 109–116, 1962. doi:10.1002/ar.1091440205.
31. **Basmajian JV.** Control and training of individual motor units. *Science* 141: 440–441, 1963. doi:10.1126/science.141.3579.440.
32. **Formento E**, **Botros P**, **Carmena JM.** Skilled independent control of individual motor units via a non-invasive neuromuscular-machine

Downloaded from journals.physiology.org/journal/jn (062.036.043.138) on June 24, 2026.

interface. *J Neural Eng* 18: 066019, 2021. doi:10.1088/1741-2552/ac35ac.
33. **Pasquet B**, **Carpentier A**, **Duchateau J.** Change in muscle fascicle length influences the recruitment and discharge rate of motor units during isometric contractions. *J Neurophysiol* 94: 3126–3133, 2005. doi:10.1152/jn.00537.2005.
34. **Wagman IH**, **Pierce DS**, **Burger RE.** Proprioceptive influence in volitional control of individual motor units. *Nature* 207: 957–958, 1965. doi:10.1038/207957a0.
35. **Negro F**, **Muceli S**, **Castronovo AM**, **Holobar A**, **Farina D.** Multi-channel intramuscular and surface EMG decomposition by convolutive blind source separation. *J Neural Eng* 13: 026027, 2016. doi:10.1088/1741-2560/13/2/026027.
36. **Lee MD**, **Wagenmakers EJ.** *Bayesian Cognitive Modeling: a Practical Course*. Cambridge University Press, 2014.
37. **van Doorn J**, **Ly A**, **Marsman M**, **Wagenmakers EJ.** Bayesian rank-based hypothesis testing for the rank sum test, the signed rank test, and Spearman's ρ. *J Appl Stat* 47: 2984–3006, 2020. doi:10.1080/02664763.2019.1709053.
38. **van den Bergh D**, **van Doorn J**, **Marsman M**, **Draws T**, **van Kesteren EJ**, **Derks K**, **Dablander F**, **Gronau QF**, **Kucharský Š**, **Gupta AR**, **Sarafoglou A**, **Voelkel JG**, **Stefan A**, **Ly A**, **Hinne M**, **Matzke D**, **Wagenmakers EJ.** A tutorial on conducting and interpreting a Bayesian ANOVA in JASP. *Annee Psychol* 120: 73–96, 2020. doi:10.3917/e.anpsy1.201.0073.
39. **Rouder JN**, **Morey RD**, **Speckman PL**, **Province JM.** Default Bayes factors for ANOVA designs. *J Math Psychol* 56: 356–374, 2012. doi:10.1016/j.jmp.2012.08.001.
40. **van den Bergh D**, **Wagenmakers EJ**, **Aust F.** Bayesian repeated-measures analysis of variance: an updated methodology implemented in JASP. *Adv Methods Pract Psychol Sci* 6: 25152459231168024, 2023. doi:10.1177/25152459231168024.
41. **Westfall PH.** Multiple testing of general contrasts using logical constraints and correlations. *J Am Stat Assoc* 92: 299–306, 1997. doi:10.1080/01621459.1997.10473627.
42. **Mulder J**, **Williams DR**, **Gu X**, **Tomarken A**, **Böing-Messing F**, **Olsson-Collentine A**, **Meijerink M**, **Menke J**, **van Aert R**, **Fox JP**, **Hoijtink H**, **Rosseel Y**, **Wagenmakers EJ**, **van Lissa C.** BFpack: flexible Bayes factor testing of scientific theories in R. *J Stat Soft* 100: 1–63, 2021. doi:10.18637/jss.v100.i18.
43. **Johnson RA**, **Wichern DW.** *Applied Multivariate Statistical Analysis*. Pearson Prentice Hall, 2007.
44. **Binder MD**, **Powers RK**, **Heckman CJ.** Nonlinear input-output functions of motoneurons. *Physiology (Bethesda)* 35: 31–39, 2020. doi:10.1152/physiol.00026.2019.
45. **Keen DA**, **Fuglevand AJ.** Common input to motor neurons innervating the same and different compartments of the human extensor digitorum muscle. *J Neurophysiol* 91: 57–62, 2004. doi:10.1152/jn.00650.2003.
46. **Büdingen HJ**, **Freund HJ.** The relationship between the rate of rise of isometric tension and motor unit recruitment in a human forearm muscle. *Pflugers Arch* 362: 61–67, 1976. doi:10.1007/BF00588682.
47. **Stotz PJ**, **Bawa P.** Motor unit recruitment during lengthening contractions of human wrist flexors. *Muscle Nerve* 24: 1535–1541, 2001. doi:10.1002/mus.1179.
48. **Holobar A**, **Minetto MA**, **Botter A**, **Negro F**, **Farina D.** Experimental analysis of accuracy in the identification of motor unit spike trains from high-density surface EMG. *IEEE Trans Neural Syst Rehabil Eng* 18: 221–229, 2010. doi:10.1109/TNSRE.2010.2041593.
49. **Farina D**, **Holobar A**, **Merletti R**, **Enoka RM.** Decoding the neural drive to muscles from the surface electromyogram. *Clin Neurophysiol* 121: 1616–1623, 2010. doi:10.1016/j.clinph.2009.10.040.
50. **De Luca CJ**, **Adam A**, **Wotiz R**, **Gilmore LD**, **Nawab SH.** Decomposition of surface EMG signals. *J Neurophysiol* 96: 1646–1657, 2006. doi:10.1152/jn.00009.2006.
51. **Brouwer B**, **Ashby P.** Corticospinal projections to lower limb motoneurons in man. *Exp Brain Res* 89: 649–654, 1992. doi:10.1007/BF00229889.
52. **de Noordhout AM**, **Rapisarda G**, **Bogacz D**, **Gérard P**, **De Pasqua V**, **Pennisi G**, **Delwaide PJ.** Corticomotoneuronal synaptic connections in normal man: an electrophysiological study. *Brain* 122: 1327–1340, 1999. doi:10.1093/brain/122.7.1327.
53. **d'Avella A**, **Saltiel P**, **Bizzi E.** Combinations of muscle synergies in the construction of a natural motor behavior. *Nat Neurosci* 6: 300–308, 2003. doi:10.1038/nn1010.
54. **Desnedt HE**, **Gidaux E.** Spinal motoneuron recruitment in man: rank deordering with direction but not with speed of voluntary movement. *Science* 214: 933–936, 1981. doi:10.1126/science.7302570.
55. **Tanzarella S**, **Muceli S**, **Santello M**, **Farina D.** Synergistic organization of neural inputs from spinal motor neurons to extrinsic and intrinsic hand muscles. *J Neurosci* 41: 6878–6891, 2021. doi:10.1523/JNEUROSCI.0419-21.2021.
56. **Schmied A**, **Vedel JP**, **Pagni S.** Human spinal lateralization assessed from motoneurone synchronization: dependence on handedness and motor unit type. *J Physiol* 480: 369–387, 1994. doi:10.1113/jphysiol.1994.sp020367.
57. **Fuglevand AJ**, **Lester RA**, **Johns RK.** Distinguishing intrinsic from extrinsic factors underlying firing rate saturation in human motor units. *J Neurophysiol* 113: 1310–1322, 2015. doi:10.1152/jn.00777.2014.
58. **Moritz CT**, **Barry BK**, **Pascoe MA**, **Enoka RM.** Discharge rate variability influences the variation in force fluctuations across the working range of a hand muscle. *J Neurophysiol* 93: 2449–2459, 2005. doi:10.1152/jn.01122.2004.
59. **Lee RH**, **Heckman CJ.** Bistability in spinal motoneurons in vivo: systematic variations in persistent inward currents. *J Neurophysiol* 80: 583–593, 1998. doi:10.1152/jn.1998.80.2.583.
60. **Heckmann CJ**, **Gorassini MA**, **Bennett DJ.** Persistent inward currents in motoneuron dendrites: implications for motor output. *Muscle Nerve* 31: 135–156, 2005. doi:10.1002/mus.20261.
61. **Lee RH**, **Heckman CJ.** Adjustable amplification of synaptic input in the dendrites of spinal motoneurons in vivo. *J Neurosci* 20: 6734–6740, 2000. doi:10.1523/JNEUROSCI.20-17-06734.2000.
62. **Lee RH**, **Heckman CJ.** Bistability in spinal motoneurons in vivo: systematic variations in rhythmic firing patterns. *J Neurophysiol* 80: 572–582, 1998. doi:10.1152/jn.1998.80.2.572.
63. **Zero AM**, **Kirk EA**, **Hali K**, **Rice CL.** Firing rate trajectories of human motor units during isometric ramp contractions to 10, 25 and 50% of maximal voluntary contraction. *Neurosci Lett* 762: 136118, 2021. doi:10.1016/j.neulet.2021.136118.
64. **Sadtler PT**, **Quick KM**, **Golub MD**, **Chase SM**, **Ryu SI**, **Tyler-Kabara EC**, **Yu BM**, **Batista AP.** Neural constraints on learning. *Nature* 512: 423–426, 2014. doi:10.1038/nature13665.
65. **Oby ER**, **Golub MD**, **Hennig JA**, **Degenhart AD**, **Tyler-Kabara EC**, **Yu BM**, **Chase SM**, **Batista AP.** New neural activity patterns emerge with long-term learning. *Proc Natl Acad Sci USA* 116: 15210–15215, 2019. doi:10.1073/pnas.1820296116.
66. **Berger DJ**, **Gentner R**, **Edmunds T**, **Pai DK**, **d'Avella A.** Differences in adaptation rates after virtual surgeries provide direct evidence for modularity. *J Neurosci* 33: 12384–12394, 2013. doi:10.1523/JNEUROSCI.0122-13.2013.
67. **Berger DJ**, **Borzelli D**, **d'Avella A.** Task space exploration improves adaptation after incompatible virtual surgeries. *J Neurophysiol* 127: 1127–1146, 2022. doi:10.1152/jn.00356.2021.
68. **Rosenkranz K**, **Williamon A**, **Rothwell JC.** Motorcortical excitability and synaptic plasticity is enhanced in professional musicians. *J Neurosci* 27: 5200–5206, 2007. doi:10.1523/JNEUROSCI.0836-07.2007.
69. **Hu N**, **Avela J**, **Kidgell DJ**, **Piirainen JM**, **Walker S.** Modulations of corticospinal excitability following rapid ankle dorsiflexion in skill- and endurance-trained athletes. *Eur J Appl Physiol* 122: 2099–2109, 2022. doi:10.1007/s00421-022-04981-9.
70. **Martinez-Valdes E**, **Negro F**, **Laine CM**, **Falla D**, **Mayer F**, **Farina D.** Tracking motor units longitudinally across experimental sessions with high-density surface electromyography. *J Physiol* 595: 1479–1496, 2017. doi:10.1113/JP273662.

Downloaded from journals.physiology.org/journal/jn (062.036.043.138) on June 24, 2026.